2016

Plasma Treatment of Zinc Oxide Thin Film and Temperature Sensing Using the Zinc Oxide Thin Film

Al-Ahsan Talukder
South Dakota State University, alahsan.talukder@jacks.sdstate.edu

PLASMA TREATMENT OF ZINC OXIDE THIN FILM AND TEMPERATURE SENSING USING THE ZINC OXIDE THIN FILM

BY

AL-AHSAN TALUKDER

A thesis submitted in partial fulfillment of the requirements for the

Master of Science

Major in Electrical Engineering

South Dakota State University

2016

PLASMA TREATMENT OF ZINC OXIDE THIN FILM AND TEMPERATURE SENSING USING THE ZINC OXIDE THIN FILM

This thesis is approved as a creditable and independent investigation by a candidate for the Master of Science degree and is acceptable for meeting the thesis requirements for this degree. Acceptance of this thesis does not imply that the conclusions reached by the candidate are necessarily the conclusions of the major department.

Qi Hua Fan, Ph.D. Date
Thesis Advisor

Steven Hietpas, Ph.D. Date
Head, Department of Electrical
Engineering and Computer Science

Dean, Graduate School Date

ACKNOWLEDGEMENTS

This thesis work was supported by Department of Electrical Engineering and Computer Science, South Dakota State University.

I would like to express my gratitude to Dr. Qi Hua Fan for providing me an opportunity to work as a graduate research assistant at his research group in South Dakota State University. I appreciate his guidance and encouragement throughout the course of my research work. I am grateful to our group's alumni, Jyotshna Pokharel for her guidance and directions during the beginning of my research work. I would like to thank Dr. Maheshwar Shrestha, Yamini Mohan, and Ishop Amatya for their cordial support during this journey.

I would also like to thank my family members back in Bangladesh for their love and support.

TABLE OF CONTENTS

LIST OF FIGURES

LIST OF TABLES

ABSTRACT

PLASMA TREATMENT OF ZINC OXIDE THIN FILM AND TEMPERATURE SENSING USING THE ZINC OXIDE THIN FILM

AL-AHSAN TALUKDER

2016

Zinc oxide is a direct and wide bandgap, II-VI semiconductor. It has large exciton binding energy, large piezoelectric constant, strong luminescence, and high thermal conductivity. These properties make zinc oxide as a suitable material for various optoelectronic applications. Vacuum based processes of fabrication of zinc oxide thin film dominate the market for their better electrical and optical properties. In this work, zinc oxide thin films were prepared by easy and low cost solution method with oriented crystal growth along (002) plane. To improve electrical and optical property of the fabricated zinc oxide thin films, films were treated with oxygen, hydrogen, and nitrogen plasmas. Oxygen plasma treatment improved the crystallinity of zinc oxide thin film. Hydrogen plasma treatments were found very effective in improving the electrical conductivity of the film sacrificing film's transmittance. Nitrogen plasma treatment following hydrogen plasma treatment could restore the transmittance maintaining the improved electrical property. Sequential oxygen, hydrogen, and nitrogen plasma treatment decreased the resistivity of zinc oxide thin film by more than two order maintaining transmittance close to the as deposited film. This work also reports a temperature sensor based on the temperature-dependent bandgap of zinc oxide semiconductors. Transmittance measurement of the ZnO films at different temperatures showed sharp absorption edge at around 380 nm and red shift characteristics. An optical

temperature sensor was established using the zinc oxide coated glass as sensing element, ultra-violet light emitting diode as light source, and a ultra-violet photodiode as light detector. Short circuit current of the photodiode was measured over a range of the zinc oxide film's temperature. The short circuit current decreased linearly with the increase of the temperature and the sensitivity was ~0.1 μA/°C.

CHAPTER 1. INTRODUCTION

1.1. Background

Zinc oxide is a very promising compound semiconductor material. It has a direct and wide bandgap of 3.37 eV at room temperature which enables it to be used in various optoelectronic applications including light-emitting diodes, laser diodes and photodetectors working in blue/UV region of electromagnetic spectrum [1, 2]. Its large exciton binding energy of 60 meV enables applications in exciton effect based optical devices [3, 4]. Zinc oxide is available in large single crystal which offers a greater advantage over other wide bandgap semiconductors. Growth on native substrate results zinc oxide layer with reduced defect densities, which gives better performance in various optoelectronic and photonic devices [5]. Surface property of zinc oxide thin film and nanostructure is sensitive to the exposure of different gases. This makes zinc oxide a promising material for gas and chemical sensor applications [6]. As the bandgap of zinc oxide is affected by temperature, thin film of zinc oxide can also be used in temperature sensing applications [7, 8].

Zinc oxide is increasing its demand as a material for transparent conductive oxide (TCO). TCOs are optically transparent in visible electromagnetic spectrum and electrically conductive. TCOs are used in liquid crystal displays (LCD), organic light emitting diode (OLED) displays, thin film solar cells, and touch screens [9, 10]. Indium tin oxide (ITO) is the most widely used TCO in current market for its high transmittance and conductivity. But ITO is becoming expensive for indium's scarcity in nature [10-12]. Florine tin oxide (FTO) could be an alternative of ITO for its suitable conductivity and low cost. But FTO's use is limited for its low transmittance in infrared region, current

leakage due to its structural defects. Indium doped cadmium oxide and aluminum doped zinc oxide are good replacement for ITO or FTO for their transmittance and conductance required for display, touchscreen and solar cell applications. Indium doped cadmium oxide's use is limited for cadmium's toxicity. Zinc oxide is a promising TCO material for its availability, low cost, non-toxicity, suitable optical and structural property [10, 13].

Zinc oxide thin films can be grown by various techniques including chemical vapor deposition (CVD) [14], RF magnetron sputtering [15], epitaxy [16], pulsed laser deposition (PLD) [17] and metal organic chemical vapor deposition (MOCVD) [18-20]. These techniques dominate the current market, although they are costly vacuum-based processes. Solution-based sol-gel deposition of ZnO thin films has been reported as a simple, easy and low-cost method [21-35]. Sol-gel derived nanocrystalline zinc oxide thin films suffer from relatively poor electrical and optical properties, due to the high density of carrier traps and potential barriers at grain boundaries [36]. Post treatments e.g. annealing, plasma processing can improve the quality and performance of the fabricated thin films [37-39].

Plasma is one of the four fundamental states of matter. It is ionized gas containing positive ions and free electrons in proportions resulting in more or less no overall electric charge. Plasma is typically formed at low pressures or at very high temperatures. Plasmas can have temperatures and energy densities higher than can be attained by chemical or other means. Plasmas can produce energetic active species which cause physical changes or chemical reactions that can occur only with difficulty or not at all in ordinary chemical reactions. Active species can include ultraviolet or visible photons; charged particles,

including electrons, ions, and free radicals; and highly reactive neutral species, excited atomic states, and reactive molecular fragments. Low temperature plasmas can be sustained by electron impact ionization of feed gases driven by external radio frequency power (RF) source [40].

Plasma processing has wide applications in microelectronics industries. RF plasma has been utilized for processing metallic, semiconductor, and dielectric materials in micro/nano fabrication, deposition of thin films, modification of surface properties. Without plasma assisted etching and material deposition on semiconductor wafers large scale microelectronics manufacturing would simply be unfeasible [41]. Plasma processing has also been used in tuning optical, electrical properties of transparent conductive oxides and zinc oxide thin films [37-39, 42, 43].

Conventional temperature measurement using thermocouple is based on thermoelectric effect and requires the sensor being in direct contact with the interested object [44, 45]. In many applications, electrical feedthrough is not allowed or not convenient. Hence, optical measurement of temperature which does not require electrical feedthrough is needed. Infrared temperature sensors have been used for temperature measurement [46]. As thermal emission depends on surface status and morphology, careful calibration is necessary for achieving high accuracy [46].

It is known that the electrical and optical properties of semiconductors strongly depend on temperature. The effect of temperature on the energy bandgap is of particular interest. In general, the bandgap of semiconductors decreases with increasing temperature [47]. This fundamental property leads to the potential of using semiconductors for

temperature sensing, although most semiconductor devices require small variation of bandgap in the operation temperature range. Among common semiconductors, zinc oxide (ZnO) has relatively large bandgap-temperature coefficient[7]. Zinc oxide has bandgap of 3.37 eV at room temperature [48, 49]. This leads to a sharp optical absorption edge at about 368 nm. The absorption edge exhibits red-shift with increasing temperature [50]. The bandgap-temperature coefficient of ZnO is -0.0003 eV K^{-1} [51, 52]. These properties make ZnO as an attractive material for optical temperature sensing.

1.2. Previous Work

Hydrogen can act as a shallow electron donor in several conductive oxide materials, either in interstitial positions or on an oxygen site [53, 54]. Effects of hydrogen plasma treatment on spray pyrolysis processed transparent conducting oxides were first reported by Major et al. in 1986. From X-ray photoelectron spectroscopy results they reported that hydrogen plasma could not reduce IZO films which they attributed to the presence of protective OH and OH ... O species on the surface of IZO [39].

C-axis orientated, polycrystalline ZnO films were fabricated on Pyrex glass substrate by sol-gel process and dc electrical conductivity and optical properties were investigated by Natsume et al. on 2000 [21]. Effect of air annealing temperature on electrical resistivity was experimented in temperature range 500-575 ˚C. Minimum resistivity of 28.2 Ω was obtained for annealing temperature of 525 ˚C. Films were transparent in the 400 – 1000 nm wavelength range of electromagnetic spectrum and had sharp absorption edges at 380nm. The absorption analysis revealed optical bandgap of 3.20- 3.21 eV and direct electron transition.

Hydrogen's doping characteristics in ZnO based on density functional theory was reported by Walle et al. on 2000 [53]. Generally, hydrogen acts as an amphoteric impurity: in p-type material, hydrogen incorporates as H^+ (a donor), and in n-type material as H^- (an acceptor) counteracting prevailing conductivity. But in ZnO which typically exhibits n-type conductivity, hydrogen acts as a shallow donor and increases the conductivity. These insights have important consequences and utilization of hydrogen in other oxides too.

Two years later, on 2002, Hofmann et al. experimentally proved the prediction of Van de Walle [Phys. Rev. Lett. 85, 1012 (2000)] by electron paramagnetic resonance (EPR) and electron nuclear double resonance (ENDOR) spectroscopy measurements [55]. EPR and Hall measurements showed the presence of two donors (D1 and D2) in nominally undoped ZnO single crystals. It was found that one of the two observed donor resonances was related to hydrogen. The concentration of hydrogen donor in commercially available ZnO was reported to be $(6\pm2) \times 10^{16}$ cm^{-3}.

The effect of hydrogen and other dopants (Al, Li, and 3d transitional metals) on the conductivity of zinc oxide film was investigated through ac impedance spectroscopy by Zhou et al. on 2004 [56]. Aluminum doping of ZnO increased the dc conductivity by about two orders. Lithium acted as acceptor and Li doping decreased the intrinsic n-type carrier density hence reduced the conductivity of the ZnO film. It was also found that 3d transitional metals (Mn, Co, and Cu) doping decreased the conductivity where Cu doping decreased the conductivity most i.e. two orders lower than the undoped ZnO. Hydrogen doping was done by ion implantation method. Hydrogen doping increased conductivity of

ZnO by four orders i.e. from 5E-2 to 350 $\Omega^{-1}cm^{-1}$. Effects of hydrogen dopant on film's structural and optical property were not reported.

Nitrogen doped p-type zinc oxide films were grown using high-vacuum plasma-assisted chemical vapor deposition method by Barnes et al. in 2005[57]. Films were (002) oriented and nitrogen doping concentration range was 0-2%. XRD measurement revealed that lattice constant decreased with increasing nitrogen doping concentration. P-type conductivity was confirmed for high doping level by both Seebeck and Hall measurements. The p-type conductivity was unstable and films became n-type after several days.

Effects of oxygen plasma on surface composition and work function of radio frequency magnetron sputtered zinc oxide films were reported by Kuo et.al in 2012. Oxygen plasma treatment resulted in an electronegative surface and an associated dipole moment, which increased the work function of ZnO from 3.74 eV to 4.21 eV [42]. Effects of oxygen plasma on optical and electrical properties of zinc oxide films were not reported.

On 2014, Morales-Masis et al. reported improved conductivity in amorphous aluminum doped zinc tin oxide (a-ZTO:Al) thin films by hydrogen plasma treatment. They showed that hydrogen plasma treatment reduced the resistivity of RF magnetron sputtered a-ZTO:Al films by 57% and increased the absorbance by only 2% [58]. These works insinuated the possibility of improving electrical properties of sol-gel processed ZnO by H_2 plasma treatment.

A transmission-type fiber optic temperature sensor was reported on 2010 [50]. The sensor was made by depositing ZnO thin film onto sapphire fiber-ending, which was set in the region to be measured. Light from a white light source passed along a multimode optical fiber and reached a graded index lens where the light got collimated and then travelled through the sapphire fiber and ZnO sensing element. Then the light was again focused by another graded index lens to the output multimode optical fiber. The output light from the multimode optical fiber was detected by an optical spectroscope. That transmission type fiber optic sensor had a resolution of 2 °C.

A reflection-type fiber optic temperature sensor using ZnO thin film was reported on 2014 [59]. That reflection type sensor's main part was a sensing head, which was made up of a convex lens, a metal tube, and a cone type sapphire prism. The sensing head was connected to a coupling fiber end. Light from a LED source of wavelength 350-450 nm was first injected to the coupling fiber. Light passed along the fiber and reached the sensing head, reflected back in ZnO coated cone prism, and again travelled along another branch of fiber which was coupled to a fiber-optical spectroscope. For these ZnO-based sensors the main sensing part had physical contact with other parts of the sensing system. Furthermore, the bandgap of insulators (e.g. optical fiber) is also expected to change with temperature. No previous studies tried to identify and/or distinguish the effects from the ZnO and the support material (e.g. optical fiber).

1.3. Motivation

Need for improved electrical properties of zinc oxide thin films maintaining good optical and structural properties. Need for an optical temperature measurement scheme requiring no electrical feedthrough or direct contact.

1.4. Objective

Fabricate zinc oxide thin film by easy and low cost solution based sol-gel process. Investigate whether plasma processing can improve opto-electronic properties of sol-gel derived zinc oxide thin film. In addition, develop a zinc oxide based optical temperature sensor. For accomplishing the objectives, following tasks were completed.

1. Fabricate zinc oxide thin film on glass substrate by easy and low cost solution based sol-gel process.
2. Treat the zinc oxide thin films by oxygen, hydrogen, and nitrogen plasma to improve film's opto-electronic properties.
3. Investigate the temperature dependent red-shift property of absorption edge of zinc oxide film and develop an optical temperature sensor.

CHAPTER 2. THEORY

2.1. Properties of zinc oxide

2.1.1. Optical properties of zinc oxide

Transmittance of a zinc oxide film depends upon the fabrication condition, impurity and defect density, and thickness of the film. The percentage transmittance of any thin film is related to its thickness (t) and absorption co-efficient (α) by following equation;

$$\%T = 10^{-\alpha t} \times 100 \tag{2.1}$$

Higher the thickness of the film, lower the transmittance of the film. Zinc oxide films can be prepared with transmittance above 90%. Transmittance measurement of zinc oxide film shows a sharp absorption edge at 380 nm which refers to the photon energy of 3.26 eV. This absorption edge corresponds to the direct inter-band transition of electron from valance band to conduction band [5].

Zinc oxide film is doped with a metal such as Al or Ga to increase the carrier density hence the conductivity of the film. Transmission window of a transparent conductive oxide (TCO) is limited by plasma oscillation frequency and bandgap associated frequency. Plasma oscillations alternatively known as Langmuir waves refer to the rapid oscillations of the electron density in conducting media. It can be described as dielectric function's instability of the of a free electron gas. At higher frequencies of photon than the material's plasma frequency, material acts like a transparent dielectric. At lower photon frequencies than the plasma frequency material reflects or absorb the photons. Angular frequency (ω_p) of plasma oscillation is defined by following equation,

$$\omega_p = \sqrt{\left(\frac{ne^2}{m_e \varepsilon_0}\right)} \quad (2.2)$$

where, n is the number density of electrons, e is the unit charge, m_e is the mass of an electron, ε0 is the vacuum permittivity. It is usually desired to increase the conductivity hence high electron density of the film for TCO applications. As seen from Eqn. (2.2), increase of *n* will result in increased plasma frequency i.e. decreased plasma oscillation wavelength which narrows the transmission window of the TCO. Figure 2.1 shows an example transmittance and reflectance spectrum for indium tin oxide (ITO) film along with plasma frequency.

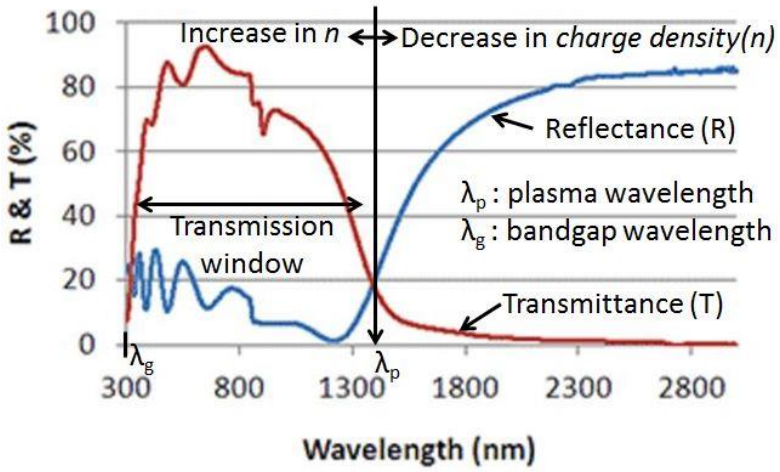

Figure 2.1. An example transmittance and reflectance spectrum for ITO film (modified [60]).

2.1.2. Structural properties of zinc oxide

Group II-IV semiconductors usually crystallize in either cubic zinc blende or hexagonal wurtzite structure. Crystal structure of ZnO shares hexagonal wurtzite, cubic zinc blende, and cubic rocksalt as shown in Figure 2.2. Wurtzite structure is

thermodynamically stable at ambient conditions and thus most common. ZnO zinc-blende structure is metastable and can only be stabilized by growth on cubic substrates such as ZnS, GaAs/ZnS. ZnO rocksalt structure may be obtained at relatively high pressures usually above 10 GPa [1].

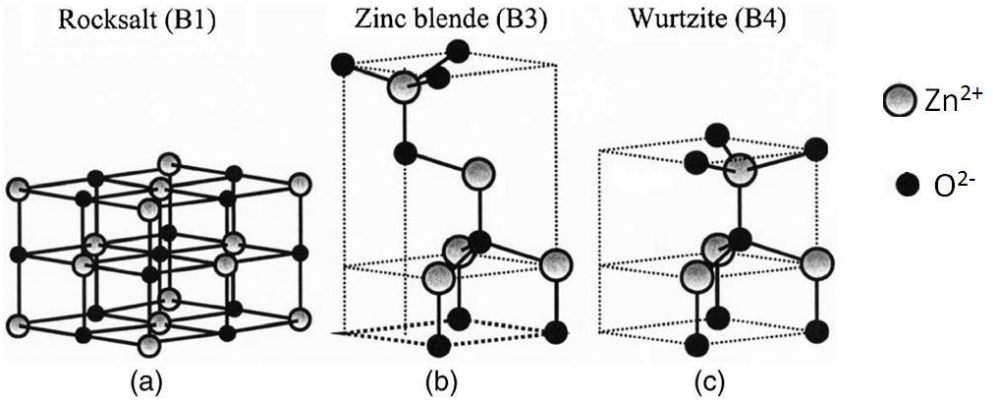

Figure 2.2. ZnO crystal structures (a) cubic rocksalt (b) cubic zinc blende, and (c) hexagonal wurtzite [1].

Figure 2.3 shows the ZnO wurtzite structure with lattice constants and bond angles. It has been that highly c-axis oriented wurtzite ZnO films could be synthesized on silicon, glass or sapphire substrate. Hexagonal ZnO wurtzite unit cell has lattice constants ranging from 3.2475 to 3.2501 Å for the *a* parameter and from 5.2042 to 5.2075 Å for the *c* parameter [1]. The bonding of ZnO is mostly ionic (Zn^{2+} and O^{2-}) with catine and anion radii of 0.074 nm and 0.140 nm respectively which accounts for preferential formation of wurtzite structure and strong piezoelectricity in ZnO.

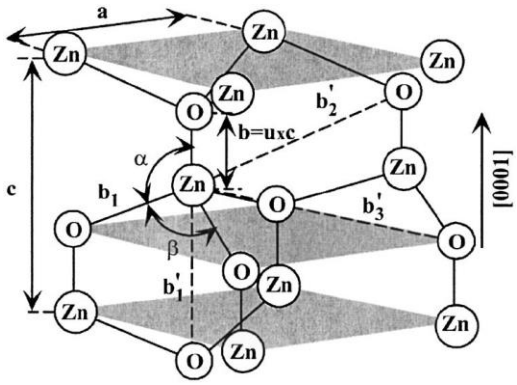

Figure 2.3. Wurtzite ZnO structure with lattice constants: a = 3.25 Å and c = 5.2 Å, bond angles: α and β (=109.47˚) [1].

2.1.3. Electrical properties of zinc oxide

Zinc oxide has relative large-direct bandgap of ~3.3 eV at room temperature. This large bandgap of facilitate use of zinc oxide for breakdown voltages, lower electronic noise, ability to sustain large electric fields, and high-power and high-temperature operation. The bandgap of zinc oxide can be tuned by alloying with MgO and CdO. Adding of Mg increases the bandgap whereas Cd decreases the bandgap of ZnO. Undoped zinc oxide has n-type conductivity. Cause of this n-type conductivity has been debated for long time. It has been postulated that n-type conductivity comes from oxygen vacancies or zinc interstitials in zinc oxide structure [61-64]. But recent density functional calculations proved that oxygen vacancies and zinc interstitials in zinc oxide are deep donors hence cannot contribute to the conductivity of ZnO [53]. This has also been experimentally proved by electron paramagnetic resonance (EPR) and Hall measurements that oxygen vacancies cannot contribute to conductivity rather the interstitial and substitutional hydrogen act as shallow donor and contribute the n-type conductivity of ZnO [55]. N-type conductivity of ZnO can be enhanced by substituting

Zn atom with group-III (e.g. Al, Ga, In) or by substituting O atom with group-VII elements (e.g. Cl or I) [65]. Resistivity of zinc oxide is related to carrier mobility and concentration in zinc oxide by following equation,

$$\rho = \frac{1}{ne\mu} \tag{2.3}$$

where n is carrier density, μ is carrier mobility, e is charge of electron and ρ is the resistivity of zinc oxide.

Reproducible, stable, and consistent p-type doping of zinc oxide has been proved to be a difficult task [1]. P-type doping is tough because of the presence of high-density shallow donors and defects such as oxygen vacancy which is no longer considered shallow donor but still act as compensation center for p-type dopants. P-type doping of ZnO can be accomplished by group-I elements such as Li, Na, K; group-V elements such as N, P and As. Cu and Ag can also be used to achieve p-type doping of ZnO. However many of these dopants are deep acceptors and cannot contribute to p-type conductivity of ZnO [48]. Though fabrication of p-type ZnO has been reported, reproducible, long lasting, and consistent p-n junction has not yet been realized [66-68].

2.2. Fabrication of zinc oxide film

2.2.1. Sol-gel process

Sol-gel process is a wet-chemical technique for producing solid materials from small molecules. This process is usually used for fabrication of metal oxides. In this process, the sol (or solution) gradually evolves toward a gel-like network comprising both a liquid phase and a solid phase [69]. Sol-gel process of thin film deposition has

many advantages over other techniques. It allows easy control over the chemical composition of the precursor solution. It is also low temperature process and it offers high yield, fast throughput roll to roll fabrication of various organic and inorganic thin films [69]. Sol-gel process of ZnO fabrication requires three basic steps: (i) solution preparation, (ii) coating and (iii) heat treatment. The precursor solution can be coated on the substrate using different method such as dip coating, spin coating or spray technique. Figure 2.4 shows a schematic diagram of Sol-gel process involving spin coating method.

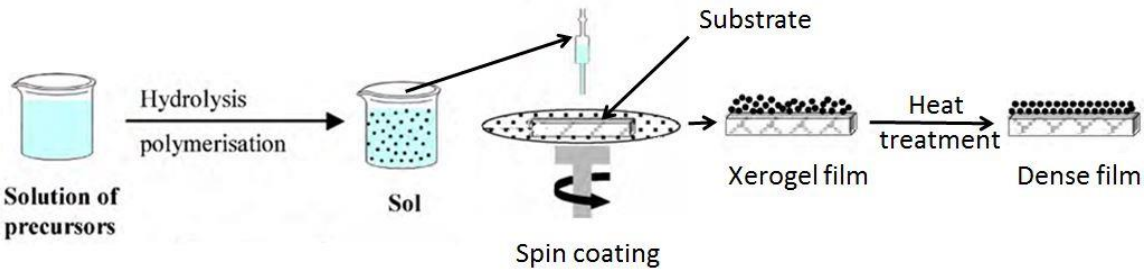

Figure 2.4. Schematic diagram of Sol-gel spin coating process [70].

2.2.2. Spin coating

Spin coating is a widely used method to deposit uniform thin film on flat substrate. A machine is used to rotate the sample in this process which is known as spin coater or spinner. In this method, the substrate is mounted on the chuck of the spin coater and the coating material is dropped at the center of the substrate which is either still or spinning at very low speed. Then the sample is spun at higher speed to spread the coating material uniformly over the substrate by centrifugal force arising from rotation of the sample. During the spinning of coated substrate, solvent evaporates and a uniform and thin layer of coating material on the substrate is formed. ZnO film of uniform thickness can be deposited using spin coating process. In this process, ZnO precursor solution is

dropped onto the substrate then the substrate is rotated usually at 2000-4000 revolutions per minute for 10-40 seconds. Higher spinning speed and longer spinning time results in thinner film. The thickness of the film also depends on the solution viscosity. Film thickness (t) is dependent upon spin speed (f), initial solution viscosity (v_0), and evaporation rate (e) by following equation: [71, 72]

$$t = f^{-2/3} {v_0}^{1/3} e^{1/3} \tag{2.4}$$

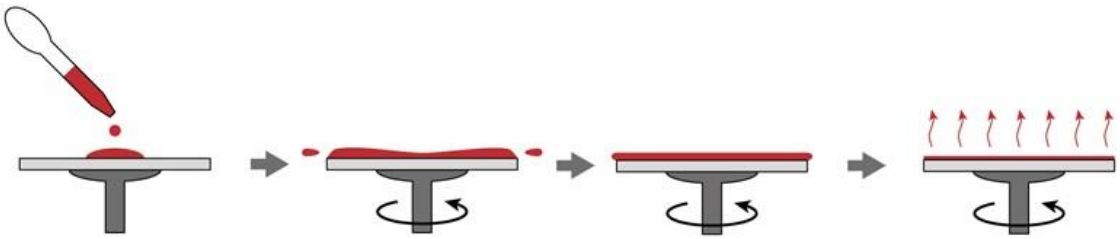

Figure 2.5. A schematic diagram of spin coating process [73].

2.2.3. Annealing

Annealing is a heat treatment of any material to alter its physical and sometime chemical changes to the material to make it more crystalline and less defective. During the annealing process the individual atoms of the material gains energy, migrate in the lattice, and reduce dislocation defects. Solution based zinc oxide thin film fabrication requires preheating and annealing of the spin coated or dip coated samples to evaporate the organic solvents and decompose zinc acetate to form zinc oxide film on the substrate. At high temperature, zinc oxide atoms crystallize in preferred orientation. Solution based zinc oxide fabrication usually requires annealing temperature equal or higher than 500 degree Celsius. Higher annealing temperature of sol-gel processed zinc oxide film results in larger crystal size [52, 74-78]. Ivanova et al. reported sol-gel derived zinc oxide film

with crystal size of 22nm for annealing temperature of 400 ˚C whereas crystal size was 40 nm for 750 ˚C annealing temperature [74]. However, very high annealing temperature can cause micro fracture and damage the film resulting increased surface roughness [77].

2.3. Capacitively coupled plasma discharge

Capacitively coupled plasma (CCP) is widely used because of its simplicity, low-pressure operation, and relatively low equipment cost. A CCP system has two electrodes separated by small distance. Feed gas is supplied at lower than atmospheric pressure. A CCP system is driven by a radio-frequency (RF) power supply which usually operates at 13.56 MHz. One of two electrodes is connected to the RF power supply, and the other one is grounded. As this configuration is alike in principle to a capacitor in an electric circuit, the configuration is called a capacitively coupled plasma system. A schematic diagram of a typical capacitively coupled plasma discharge system is shown in Figure 2.6. A matching network with variable reactive elements is added for maximum power transfer from the external power source to the plasma load.

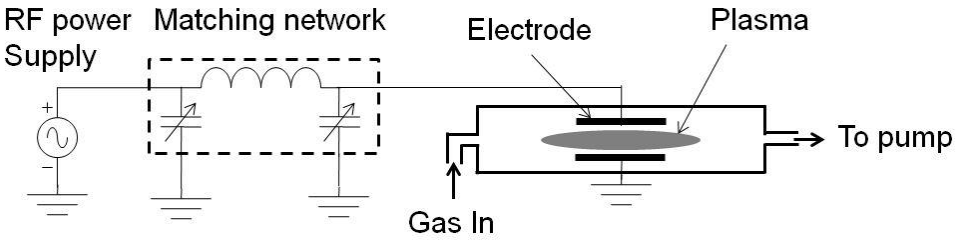

Figure 2.6. Capacitively coupled RF plasma discharge system.

When RF power is applied to the metallic electrodes, the feed gas is ionized. The applied electric field accelerates electron and gives rise to its kinetic energy. If the electric field is strong enough, the accelerated electrons hit other atoms, ionize those

atom, and produces secondary electrons. This process leads to avalanche breakdown resulting ionization of the feed gas. Some of the exited electrons recombine with the atom and lose energy in the form of visible radiation resulting glowing of the discharge. Typical electron density is ~ 10^9 – 10^{10} cm^{-3} in capacitively coupled plasma systems. RF power supply initiates and sustains the plasma discharge by providing power to the plasma [41].

2.4. Characterization of zinc oxide thin films

2.4.1. Spectrophotometer

A spectrophotometer is an optical characterization system which can determine the transmittance, absorbance, and reflectance spectrum of a sample over ultra-violate, visible, and near infra-red range of electromagnetic spectrum. As the name implies, a spectrophotometer consists of two parts; a spectrometer and a photometer. The spectrometer can produce light of any desired wavelength and the photometer can detect the intensity of any incident light of any specific wavelength. A simple schematic diagram of spectrophotometer is shown in Figure 2.7. Main parts of a spectrophotometer are a light source, a monchromator, a sample holder, and a detector. The monochromator splits the light coming from the source into individual wavelength components, and allows a single wavelength light at a time. The monochromatic light passes through the sample and incidents on the detector [79]. The detector can detect the intensity of light transmitted through the sample and give corresponding electrical signal. The software installed in the computer receives this voltage signal and gives a spectrum over wide wavelength range (e.g. 200 -1700 nm).

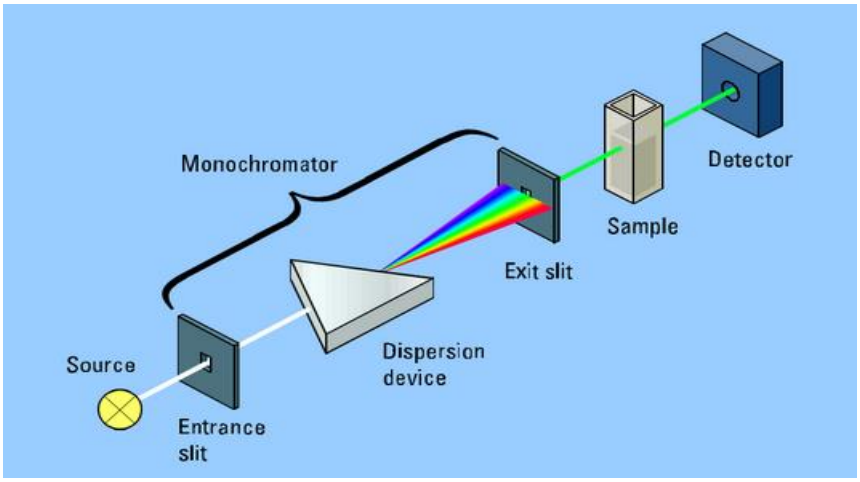

Figure 2.7. A simple schematic diagram of spectrophotometer [80].

The transmittance irradiance (I) is related to incident irradiance (I_0) by Beer Lambert law given in Eqn. 2.5 where α is the absorption coefficient and t is the thickness.

$$I = I_o 10^{-\alpha t} \tag{2.5}$$

Transmittance is the ratio of transmittance irradiance (I) is related to incident irradiance (I_0) given in Eqn. 2.6 and usually expressed in percentage (%).

$$\%T = \frac{I}{I_0} \times 100 = 10^{-\alpha t} \times 100 \tag{2.6}$$

As shown in Eqn. 2.7, absorbance A is the product of absorption coefficient, α and thickness, t of the sample.

$$A = \alpha t \tag{2.7}$$

Absorbance A is related to Transmittance T as given in Eqn. 2.8. When all the light passes through the sample without any absorption, Absorbance A is zero, and Transmittance is 100%. If all the light is absorbed, Transmittance is 0% and Absorbance is infinite [79].

$$A = \log\left(\frac{I_0}{I}\right) = \log\frac{100}{\%T} = 2 - \log(\%T) \tag{2.8}$$

2.4.2. X-ray diffraction

X-ray diffraction (XRD) is an analytical technique for phase identification of crystalline materials and used for determining crystal structure, crystallinity, lattice parameters, atomic spacing, and percent phase composition of sample under test. In XRD X-ray is used as its wavelength is comparable with the spacing of the atomic layers of crystalline sample. XRD measurements work as a fingerprint of a crystalline material. Crystalline materials contain layers of atoms arranged periodically in specific order. When monochromatic X-ray beam strike the sample, x-ray beam is scattered by atoms in different layers. Such geometry is shown in Figure 2.8. Scattered beam travels in another direction and produce constructive and destructive interference determined by Bragg's law:

$$2d \sin\theta = n\lambda \tag{2.9}$$

here, d is the spacing between diffracting planes, λ is the wavelength of the beam, θ is the incident angle, and n is any integer indicating order of diffraction.

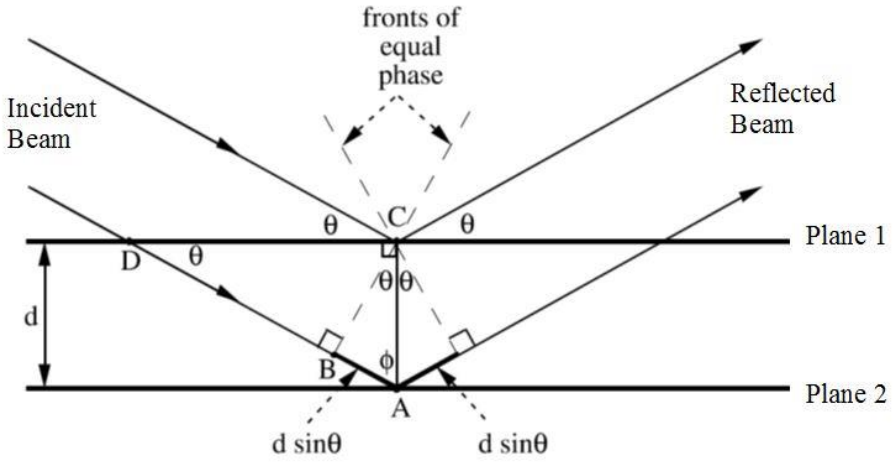

Figure 2.8. Geometry of interference of two waves scattered by two planes [81].

An X-ray diffractometer is composed three main components; an X-ray tube, a sample holder, and an X-ray detector as shown in Figure 2.9. X-ray is produced in the X-ray tube by bombarding a metal target by electron beam emitted from a hot filament. The electron beam knockout electrons from K-shell of the target material. Vacancy in the K-shell is filled by electron dropping down from L or M shell. These dropping electron emits energy in the form of X-ray having wavelength in Angstrom range. Copper is the most common target material producing x-ray having wavelength of 1.5418Å. The X-ray beam is collimated and passed through a monochromator to filter the x-ray beam of specific wavelength. The monochromatic X-ray beam is then directed to sample. Incident X-ray interacts with the atomic layers of sample which scatter the incident beam toward x-ray detector. X-ray detector detects the scattered beam of X-ray and counts the number of scattered X-rays. The arrangement of detector mounting is such that when the sample is rotated by and angle of θ from the incident beam, the detector mounted on the arm

rotates by angle of 2θ to collect the diffracted X-rays. An instrument named goniometer is used to maintain the angle and rotate the sample. [81, 82]

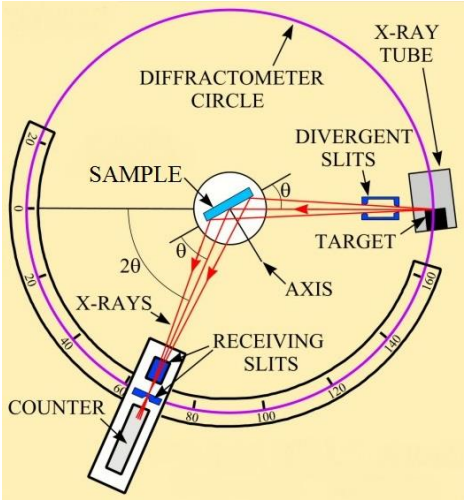

Figure 2.9. Schematic diagram of an X-ray diffractometer [82].

2.4.3. Hall Effect measurement

Hall Effect measurement is an electrical characterization method utilizing Hall Effect to determine carrier density, mobility of carriers, and electrical resistivity in semiconductors. Hall Effect is production of electric voltage difference across a flat conductor orthogonal to electrical current and a magnetic field applied perpendicular to the direction of electrical current. Figure 2.10 shows a simple illustration of Hall Effect. When a magnetic field is applied perpendicular to the direction of current flow, the carriers of the current experience a Lorentz force normal to both magnetic field and current direction and distribution of carrier becomes non uniform. The Lorentz force is a vector quantity which has magnitude and direction determined by carrier type (electron/hole), magnetic field's direction and carrier's direction. Resultant force on the carrier is,

$$\boldsymbol{F} = \boldsymbol{q}(\boldsymbol{E} + \boldsymbol{v} \times \boldsymbol{B}) \tag{2.10}$$

Where, $\boldsymbol{E}$ is the applied electric field, $\boldsymbol{v}$ is the velocity of the carriers, $\boldsymbol{q}$ is the carrier's charge, and $\boldsymbol{B}$ is the applied magnetic flux density. [83, 84]

Figure 2.10. Simple illustration of Hall Effect [84].

Hall Effect measurement can determine the carrier type based on the direction of Hall voltage. Figure 2.11 shows the direction of Hall voltages for p-type and n-type semiconductor. For p-type semiconductor majority carrier is hole. Upon application of magnetic flux density $\boldsymbol{B_z}$, Lorentz force is exerted on holes, holes are accumulated in left side of conductor and holes are depleted on right side causing a Hall voltage with positive polarity on left side of the conductor as shown in Figure 2.11 (a). For n-type semiconductor Hall voltage is produced with negative polarity on left side of the conductor as shown in Figure 2.11 (b).

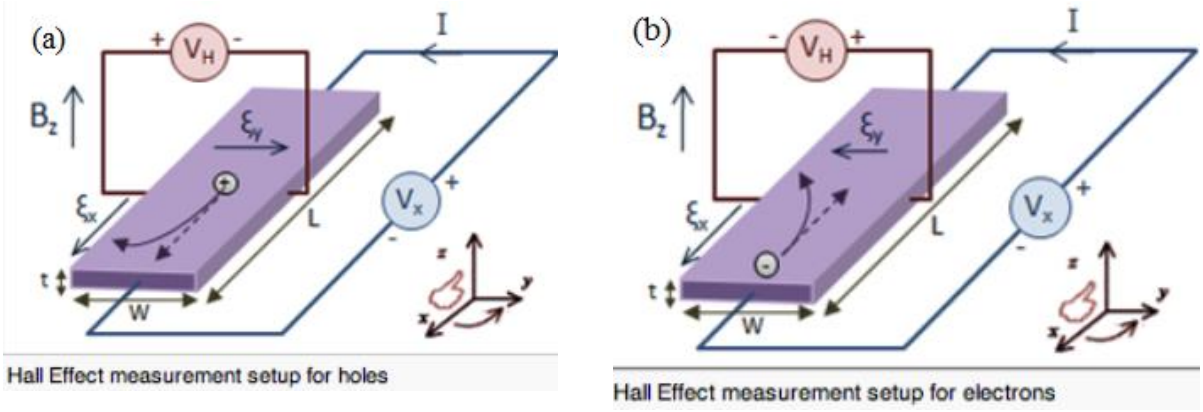

Figure 2.11. Schematic showing the Hall Effect in (a) p-type semiconductor (b) n-type semiconductor [83].

The magnitude of the Hall voltage is given by,

$$V_H = \frac{IB}{qnt} \tag{2.11}$$

Here I is the electric current, B is the Magnetic flux density, n is the carrier density and t is the conductor's thickness. Eqn. 2.7 can be used to find carrier density when all other quantities are known and measureable. Sheet density n_s is more convenient and its value isnt. Then the value of sheet density n_s is,

$$n_s = \frac{IB}{qV_H} \tag{2.12}$$

The sheet resistance R_s of the semiconductor can be determined using convenient van der Pauw resistivity measurement technique. Since sheet resistance involves sheet career density and mobility, Hall mobility can be determined from Eqn. 2.13 [85],

$$\mu = \frac{1}{qn_sR_s} = \frac{V_H}{IBR_S} \tag{2.13}$$

2.4.4. Atomic force microscopy

Atomic force microscope (AFM) is a high precision scanning probe microscope which is used in studying sample in nanoscale. Figure 2.12 shows a schematic diagram of an atomic force microscope. In AFM a tip which is 3-6 um tall pyramid with 15-40nm end radius is mounted on a cantilever. Tip is raster scanned over the sample to get the morphology of the sample. When the tip is brought close to the sample, force (*f*) between the sample and tip causes deflection (*x*) of the cantilever according to the Hooke's law,

$$f = -kx \tag{2.14}$$

where, *f*= force between tip and sample, *k* = spring constant of cantilever, and *x* = deflection of the cantilever. Deflection of the cantilever is detected by an optical arrangement. A laser beam strike is reflected off the back of the cantilever to a segmented photodetector. Whenever, the tip moves up and down following the sample surface's morphology, the position of the reflected lased point moves from set point at photodetector. This information is sent to a computer by feedback loop to control the z-axis movement of stage (piezo-scanner) to maintain constant separation and force between tip and sample. The sample is moved in x-y plane to raster scan the desired surface, and corresponding y axis movement information of the tip is recorded at the computer to construct a three dimensional morphology of the sample surface. AFM is usually operated in three different operating modes: contact mode, tapping mode, and non-contact mode [86].

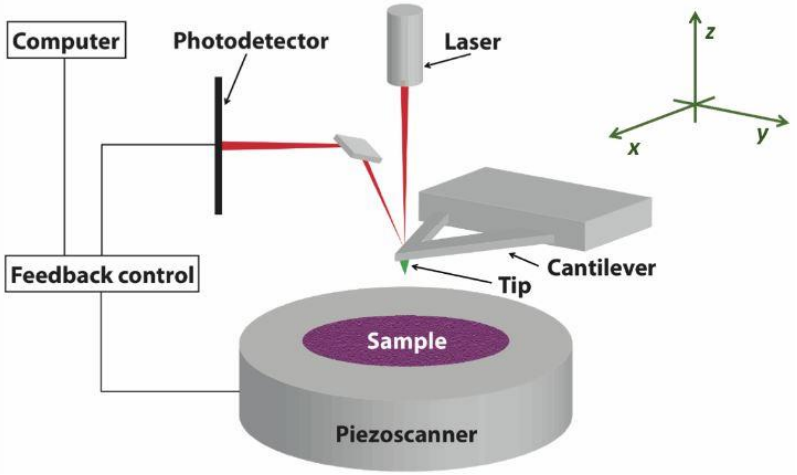

Figure 2.12. Schematic diagram of an atomic force microscope [87].

CHAPTER 3. EXPERIMENTAL PROCEDURE

3.1. Fabrication of ZnO thin film

3.1.1. Substrate Preparation

Glass slides were cut into small pieces of dimension 2.5 cm x 2.5 cm for using as substrate. Glass substrates were ultrasonically cleaned in Fisher Scientific ultrasonic bath (shown in Figure 3.1) using soapy water, deionized water, acetone and 2-propanol sequentially for 10 minutes in each solution. Then the glass slides were dried in nitrogen blow and stored in sample storing box.

Figure 3.1. Fisher scientific ultrasonic bath (model: FS20D).

3.1.2. Deposition of ZnO thin film

To prepare zinc oxide sol-gel, zinc acetate dihydrate [$Zn(CH_3COO).2H_2O$], 2-methoxethanol [$CH_3OCH_2CH_2OH$] and ethanolamine [$HOCH_2CH_2NH_2$] were used. Molar ratio of ethanolamine to zinc acetate dihydrate was 1.0 and the concentration of zinc acetate was 0.35 M. The solution was then stirred at 500 rpm for two hours followed by stirring for one more hour at 80 ˚C to evaporate organic compounds. The zinc oxide

solution was dropped onto the cleaned and dried glass substrates using pipette. The substrate was then rotated at 2500 rpm for 30 seconds using Laurell spin coater (shown in Figure 3.2) to obtain a thin film on the glass substrates. Thin film coated glass substrates were then dried in a furnace (shown in Figure 3.3) at 500 ˚C for one hour to evaporate solvent and remove organic residuals. The samples were again spin coated and dried in oven. This process was repeated ten times to get final ZnO thickness of ~200 nm on the glass substrate.

Figure 3.2. Laurell spin coater (model: WS-400B-6NPP/LITE).

Figure 3.3. Thermo Scientific furnace.

3.2. Plasma processing of ZnO thin film

The samples were treated separately with oxygen, hydrogen and nitrogen using a custom capacitive coupled RF plasma system. Simple schematic diagram of the plasma system is shown in Figure 3.4. RF power source frequency and power was maintained at 13.56 MHz and 50 watts respectively. Plasma was formed in a 50 cm long and 2 cm diameter quartz tube which was sealed in one end with rubber washer and pumped down using a roughing pump. Other end of the tube was connected to the gas cylinders via tubing and pressure gauges. Gas cylinders containing 10% O2 in Argon, 10% H2 in Argon, and pure N2 were used. The flow rate of the gas was controlled to maintain the discharge pressure at ~2 Torr.

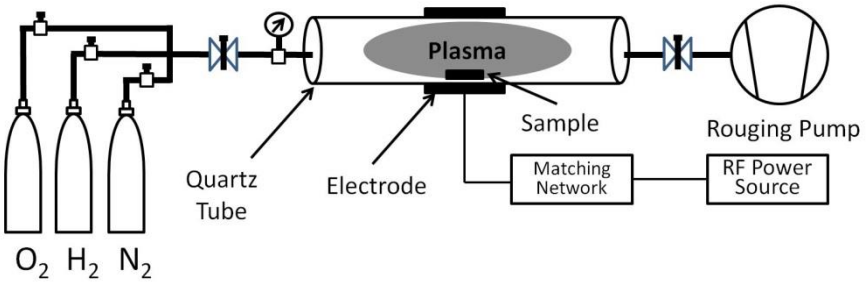

Figure 3.4. Schematic diagram of custom capacitive coupled plasma system.

3.2.1. Transmittance of plasma treated ZnO films

Optical transmittance of the ZnO samples was measured using Filmetrics F-20 spectrometer thin film analyzer with Hamamatsu (L120290) light source (shown in Figure 3.5) having combination of halogen and deuterium lamps. The light source was turned ON and 5 minutes wait time was maintained to let the light source be stable. Shutter of the source was opened to allow the light be incident on the sample. Top optical cable's distance from the sample stage was adjusted to focus the light from the fiber on

the stage surface. Filmetrics F-20 software was opened from the computer. Optics recipe was edited for transmittance measurement. The system was calibrated for 100% and 0% transmittance by removing any sample on the stage and placing an opaque sample on the stage respectively. Then the interested sample was placed on the stage, measurement was taken from the software.

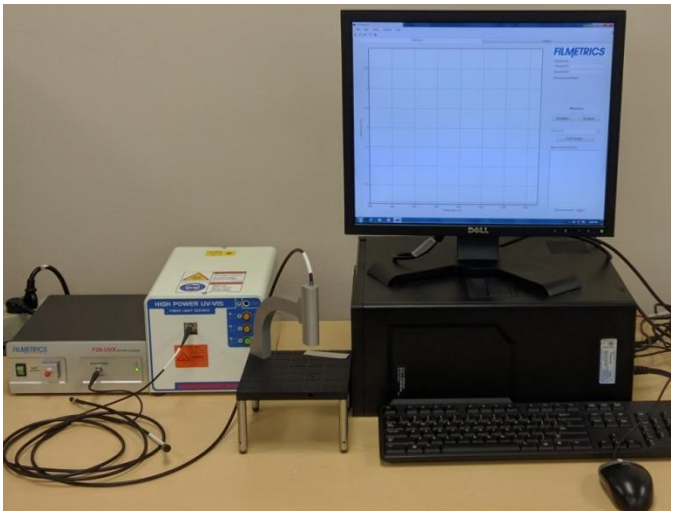

Figure 3.5. Transmittance measurement system using Filmetrics F-20 optical spectrometer.

3.2.2. XRD spectrum of plasma treated ZnO films

Crystallinity characterization of the ZnO films was carried out using Rigaku Smartlab X-ray diffractometer (XRD) shown in Figure 3.6 with Cu-Kα radiation (λ-1.54 Å). X-ray diffraction unit and CPU were turned ON. Door lock was opened, sample was place on the sample stage and door was closed. Smart-lab guidance software from the computer was used in order to measure the XRD spectrum. Startup menu was used to ramp the voltage at 40KV and current at 44mA which took 15 minutes to heat the X-Ray filament. Medium resolution PB/PSA icon was used to assign the parameters for

measurement. Angle of measurement was assigned from 20 to 80 degree at a scan rate of 0.5 degrees/min. Execute icon was used to start the measurement. FWHM values were obtained by using PDXL2 software. Shutdown button was used to reduce the filament voltage and current; sample was taken out and X-ray diffraction door was closed safely.

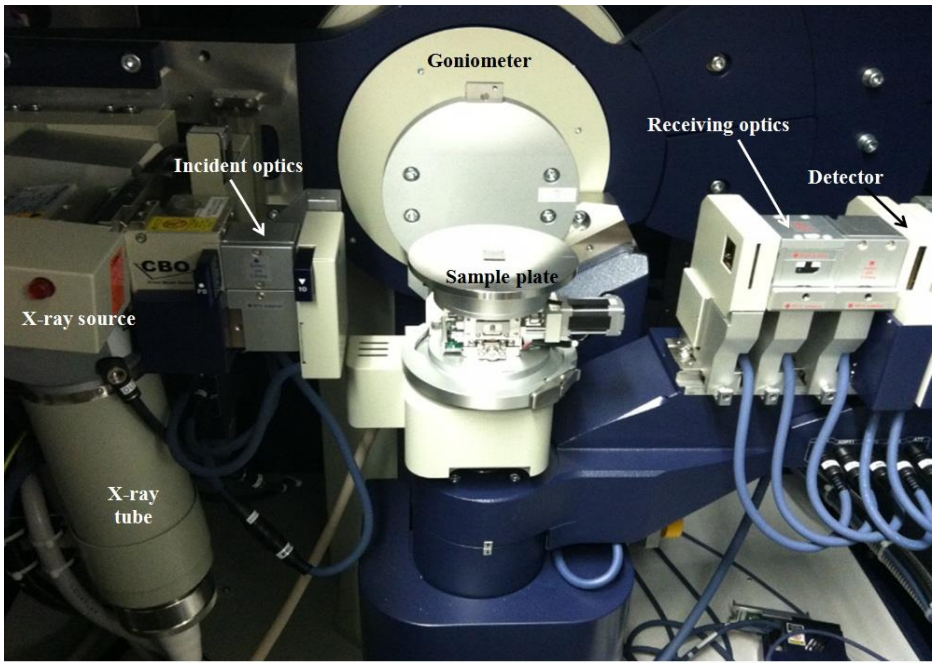

Figure 3.6. Rigaku Smartlab X-ray diffractometer [88].

3.2.3. Electrical properties of plasma treated ZnO films

HMS-3000 Ecopia Hall Effect measurement system shown in Figure 3.7 was used to measure electrical parameters- resistivity, hall mobility and carrier concentration of zinc oxide films. Ecopia Hall Effect system was turned on along with HMS-3000 software from the computer. Sample size 1 cm x 1 cm was attached to the sample board and placed in instrument's the magnetic field. The magnetic intensity and current values were set to 0.4 T and 10 mA respectively. Films mobility and carrier concentration were then obtained by pressing the measure icon on the software.

Figure 3.7. HMS-3000 Ecopia Hall Effect measurement system.

3.3. Temperature sensing using zinc oxide thin film

3.3.1. Transmittance and spectral intensity measurements

3.3.1.1. Absorption edge of zinc oxide thin film

Junction tip of K-type thermocouple (model: Agilent U1186A) was attached to zinc oxide film firmly by using a paper clip. Other end of the thermocouple was plugged to a hand held multimeter using an adaptor. Zinc oxide thin film coated glass was heated up to ~200 ˚C using hot air blower. Then the hot ZnO film coated glass was placed on the stage of Filmetrics optical spectrophotometer. Transmittance of the ZnO film coated glass was measured in the same way described in section 3.2.1. Transmittance measurements were taken when the multimeter was reading film's temperature 50 ˚C, 90 ˚C, 130 ˚C, and 170 ˚C. Independent axis (wavelength, nm) was adjusted from 365 nm to 410 nm to observe the temperature's effect on zinc oxide film's transmittance.

3.3.1.2. Absorption edge of glass substrate

Junction tip of K-type thermocouple (model: Agilent U1186A) was attached to bare glass substrate firmly by using a paper clip. Other end of the thermocouple was

plugged to a hand held multimeter using an adaptor. The glass substrate was heated up to ~200 ˚C using hot air blower. Then the hot glass substrate was placed on the stage of Filmetrics optical spectrophotometer. Transmittance of the glass substrate was measured in the same way described in section 3.2.1. Transmittance measurements were taken when the multimeter was reading glass substrate's temperature 50 ˚C, 90 ˚C, 130 ˚C, and 170 ˚C. Independent axis (wavelength, nm) was adjusted from 265 nm to 410 nm to observe the temperature's effect on glass substrate's transmittance.

3.3.1.3. Spectral Intensity distribution of the UV LED

The UV LED (model: RL5-UV0315-380) purchased from "Super Bright LED" was placed on stage of Filmetrics optical spectrophotometer. The light source of spectrophotometer measurement system was kept off. Then the UV LED was powered by 3.5 volt DC power supply. Then measurement was taken by the Filmetrics software following the procedure described in section 3.2.1 and obtained intensity spectrum was normalized in Origin software.

3.3.2. Setup for ZnO based temperature sensing

Figure 3.8 shows a schematic diagram of an experimental setup for ZnO based optical temperature sensor. A ultra-violet light emitting diode of 380 nm wavelength was powered at 3.5 volts by a DC power supply. Two convex lenses were used to focus the light emitted from the LED. ZnO coated glass was fixed on an aluminum block set inside a pair of heaters. The ceramic heaters were connected to the output terminals of a temperature controller (Omega CN38S). A thermocouple was attached to the ZnO film to calibrate the actual temperature of the ZnO film and fed to the temperature controller.

ZnO film along with the heaters setup was placed in between the convex lenses so that the UV light would focus in a small area on the ZnO film. A UV photodiode was placed at the focus point of second convex lens. The terminals of the photodiode were connected to a Fluke 289 True RMS multimeter to measure the photo-current. Using the temperature controller, the ZnO film was heated to different temperatures and corresponding photo-current was recorded. The response of the photodiode was also recorded for bare glass heated to different temperatures.

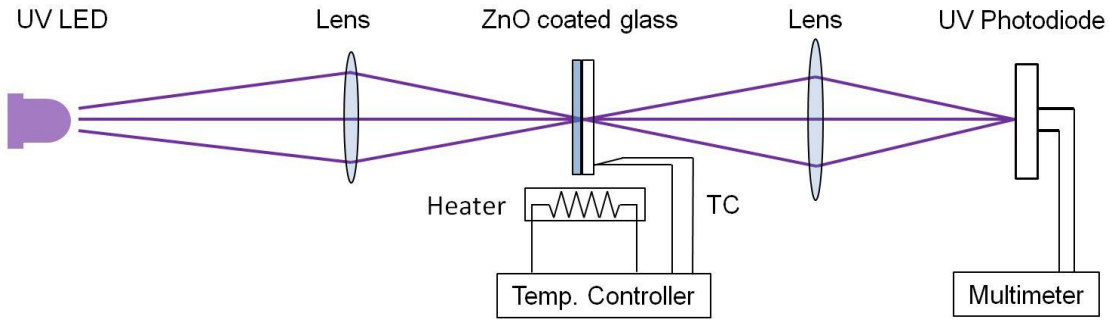

Figure 3.8. Schematic diagram of experimental setup for ZnO based optical temperature sensor.

3.3.3. Structural and morphological measurement

3.3.3.1. XRD measurement of ZnO film before and after using as sensing element

XRD measurement of as prepared zinc oxide film was done following the same procedure described in section 3.2.2. The zinc oxide film was then used in the temperature sensing system. Then the zinc oxide film was again taken back to the XRD measurement system for obtaining the XRD spectrum of the tested zinc oxide film. The XRD spectrum of as prepared and tested zinc oxide film were compared.

3.3.3.2. AFM topography of ZnO film before and after using as sensing element

BRUKER Dimension icon atomic force microscope (AFM) shown in Figure 3.9 with *ScanAsyst* software was used to characterize morphology of zinc oxide film before and after using as sensing element. 'Nanoscope 9.1' icon was double clicked to open AFM Control program. "ScanAsyst in Air" program was selected and experiment was allowed to be loaded. In the workflow toolbar, 'Align' window was opened and probe was aligned by adjusting two knobs (for X and Y movement) of the probe holder; moving the reflected laser point to the central X-Y cross point of detector indicated by maximum sum signal. Navigate window was clicked for loading focusing the sample. In navigate window, sample was loaded and stage was moved to scan position. Then the sample surface was focused by moving the stage up/down. In the engage window, proper parameters were set for scan size, aspect ratio, scan rate, X/Y offset positions, and samples/line. Then engage icon was clicked to start the scanning process and 2D & 3D topography images were saved.

Figure 3.9. *BRUKER Dimension icon* atomic force microscope.

CHAPTER 4. RESULTS AND ANALYSIS

4.1. Plasma treatment of zinc oxide thin film

4.1.1. Effect of plasma treatment on transmittance of ZnO films

4.1.1.1. Oxygen plasma treatment of zinc oxide film

Figure 4.1shows transmittances of oxygen plasma treated ZnO film. The ZnO thin films treated with oxygen plasma for, 5 minutes, 10 minutes, 20 minutes, 40 minutes and as deposited film had almost same transmittance in visible spectrum (400 nm - 700 nm). The average transmittance was around 85% in visible range of electromagnetic spectrum. Oxygen plasma treatment did not affect or worsen the transmittance of the film. A transmission edge is also noticeable in wavelength 365-385 nm which corresponds to the bandgap energy (3.40 - 3.22 eV) of zinc oxide.

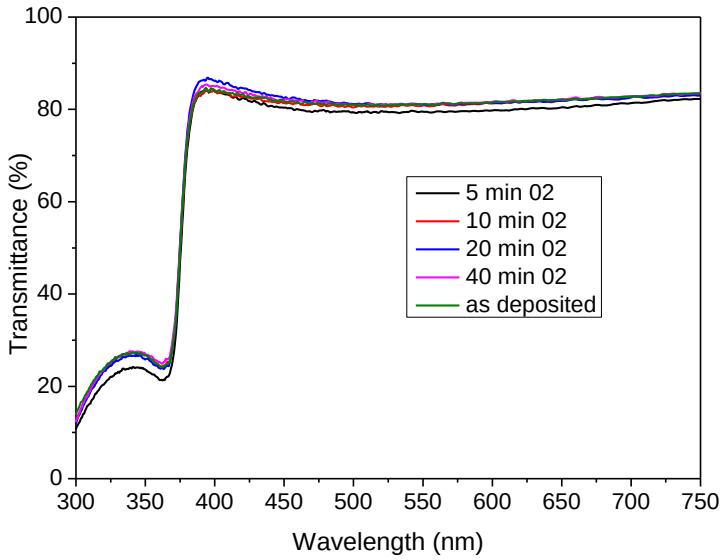

Figure 4.1 Transmittance of oxygen plasma treated ZnO film.

4.1.1.2. Hydrogen plasma treatment of zinc oxide film

Figure 4.2 shows transmittances of ZnO films treated with hydrogen plasma for 30 seconds, 1 minute, and 2 minutes. Hydrogen plasma treatment of ZnO film decreased it's transmittance in visible wavelength spectrum. As the hydrogen treatment time was increased transmittance continued to decrease. This reduction in transmittance was attributed to the creation of oxygen vacancies by hydrogen plasma. Hydrogen plasma reduced the ZnO film and created oxygen vacancies in the zinc oxide film. Each oxygen vacancy left two free electrons, which might combined with a zinc ion and formed zinc metal. Increased oxygen vacancies and formation of metal might reduce the transmittance of the film.

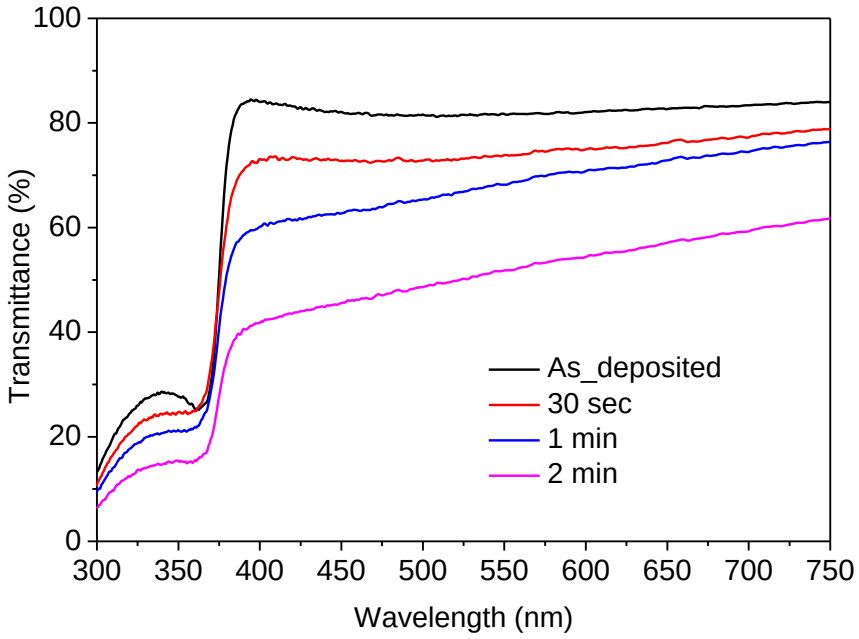

Figure 4.2. Transmittance of hydrogen plasma treated ZnO films.

4.1.1.3. Oxygen, hydrogen, and nitrogen plasma treatment of zinc oxide film

Oxygen plasma could enhance the crystallinity of as deposited film which will be shown in section 4.1.2.1. Hydrogen plasma decreased both transmittance and crystallinity of the film which will be shown in section 4.1.2.2. Beyond 30 second treatment time hydrogen plasma caused very poor optical transmittance of the film as shown in section 4.1.1.2. Hydrogen plasma treatment only for 30 second could enhance electrical property enough which will be presented in section 4.1.3. That is why for sequential plasma treatments, 20 minutes oxygen plasma was followed by 30 seconds hydrogen plasma treatment. This section will present that 20 minutes nitrogen plasma following hydrogen plasma treatment could restore the optical transmittance to ~80%. Figure 4.3 compares the transmittance spectra of the ZnO film treated with oxygen, hydrogen, and nitrogen plasmas separately and sequentially. Average transmittance over visible wavelength range (400-700 nm) for the as-deposited ZnO film, oxygen plasma treated film, and nitrogen plasma treated film were 82%, 81.3% and 81.2%, respectively, which were within 1% variation. Hydrogen plasma treated sample had the lowest transmittance having average value of 76.7% in visible wavelength spectrum. Hydrogen plasma worked as reducing agents and created oxygen vacancies, might form metal zinc, and defects in the film. The increase defects were attributed to reduce transmittance by scattering the light wave. Treatment with all three plasmas sequentially resulted in higher transmittance than hydrogen plasma treated sample. The average transmittance over visible wavelength spectrum for all plasma treated sample was 79.8%. Nitrogen plasma treatment following hydrogen plasma could overcome the adverse effect on transmittance of hydrogen plasma. Nitrogen species might form bond with preceding hydrogen plasma introduced

metal zinc. Nitrogen species might also occupied the oxygen vacancies resulting in significant improvement of transmittance.

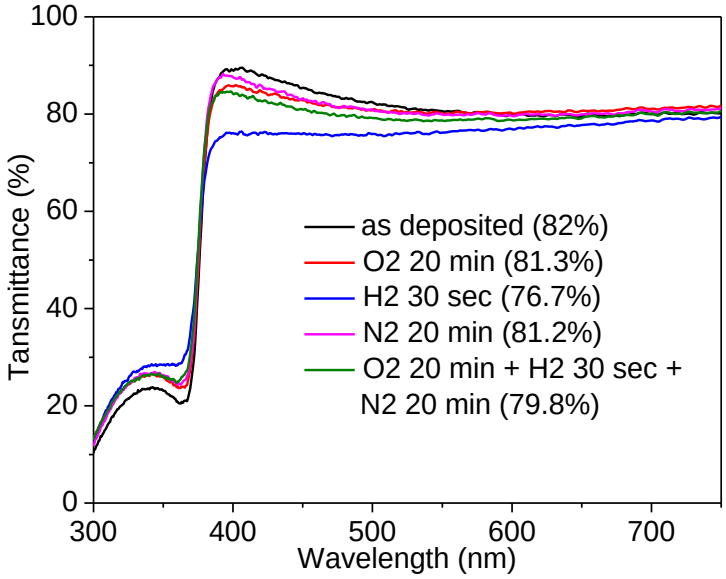

Figure 4.3. Transmittance spectra of the ZnO film treated with oxygen, hydrogen, and nitrogen plasmas separately and sequentially.

4.1.2. Effect of plasma treatment on structural property of ZnO films

4.1.2.1. Oxygen plasma treatment of zinc oxide film

Figure 4.4 shows XRD intensities of ZnO films treated with oxygen plasma. Oxygen plasma treatment did not shift the peak position (at $2\theta = 34.40$ degree) of XRD patterns of ZnO films. Table 4.1 shows FWHM values for XRD peaks of ZnO films treated with oxygen plasma. FWHM values were affected to some extent by the time of oxygen plasma treatment. Lowest FWHM value and sharpest XRD peak was found for 20 minutes oxygen plasma treated ZnO film which is supposed to have highest crystallinity. This increase in crystallinity is attributed to the making of new bond by oxygen species from plasma with interstitial Zn^{2+} ions hence expanding the grain

boundaries. Oxygen plasma might also have decreased the oxygen vacancies to improve crystallinity. Oxygen plasma treatment more than 20 minutes did not continue to sharpen the peak. Oxygen plasma treatment of 40 minutes gave higher FWHM value than that of 20 minutes treated sample. Excess oxygen plasma treatment beyond 20 minutes might have reacted and broken Zn-O bond to reduce crystal grain size.

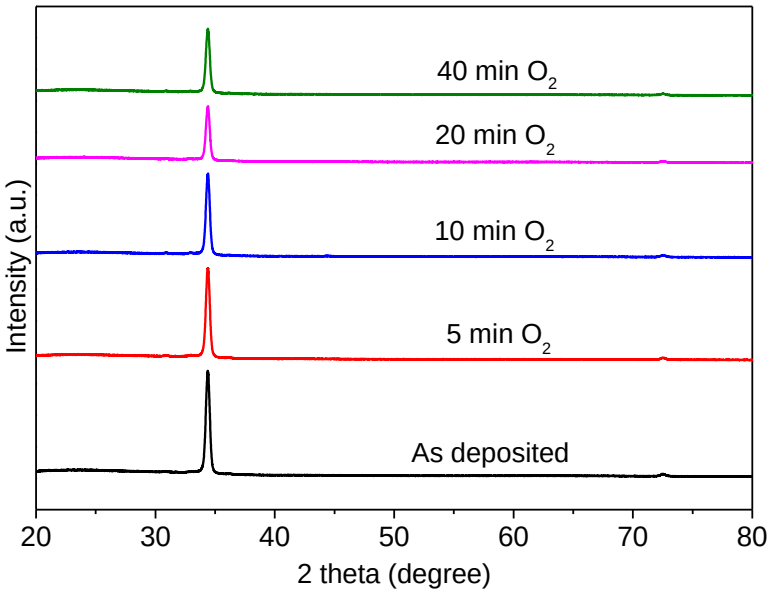

Figure 4.4. XRD intensities of ZnO films treated with oxygen plasma.

Table 4.1. FWHM values for XRD peaks of ZnO films treated with oxygen plasma

Oxygen plasma condition	As deposited	5 min oxygen	10 min oxygen	20 min oxygen	40 min oxygen
FWHM	0.3639	0.3603	0.3585	0.3567	0.3652

4.1.2.2. Hydrogen plasma treatment of zinc oxide film

Figure 4.5 shows XRD intensities of ZnO films treated with hydrogen plasma for 30 seconds, 1 minute, and 2 minutes. Maximum peak intensity was observed for as deposited film and peak intensity continued to decrease with increasing hydrogen plasma treatment time. This was attributed to the increased oxygen vacancies. As stated earlier, hydrogen plasma adsorbed oxygen species from the ZnO film and decreased the crystallinity of the ZnO film. Table 4.2 shows FWHM values for XRD peaks of ZnO films treated with hydrogen plasma for 30 seconds, 1 minute, and 2 minutes. With increasing time of hydrogen plasma treatment, FWHM value increased indicating reduced crystallinity.

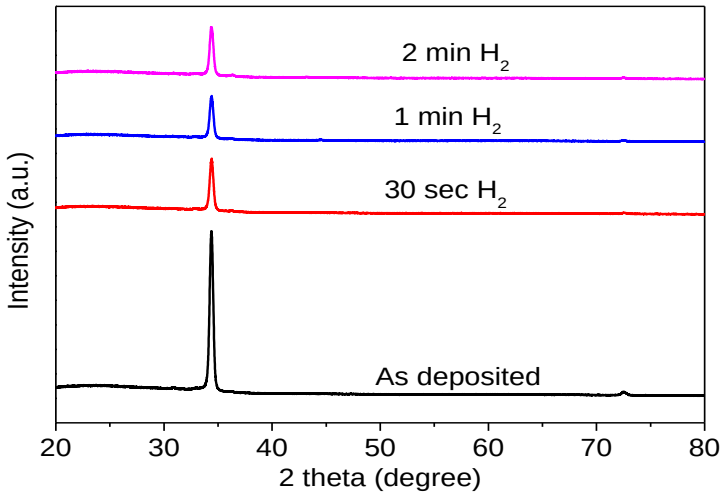

Figure 4.5 XRD intensities of ZnO films treated with hydrogen plasma.

Table 4.2. FWHM values for XRD peaks of ZnO films treated with hydrogen plasma.

H2 plasma condition	As deposited	30 seconds hydrogen	1 minute hydrogen	2 minutes hydrogen
FWHM	0.3639	0.3695	0.3847	0.3777

4.1.2.3. Oxygen, hydrogen, and nitrogen plasma treatment of zinc oxide film

Figure 4.6 shows XRD intensity patterns for ZnO film treated with oxygen, hydrogen, nitrogen plasma. Table III shows FWHM values for oxygen, hydrogen and nitrogen plasma treated ZnO films. As-deposited film had FWHM value of 0.3639. Oxygen treated ZnO film had the lowest FWHM value of 0.3567 which indicated maximum crystal size for oxygen plasma treated film. Oxygen plasma treatment reduced the oxygen vacancies and made new Zn-O bond with interstitial zinc atom in film hence increased the crystallinity of the film. Hydrogen plasma treatment increased the FWHM value to 0. 3695 which indicated reduced crystallinity. Hydrogen plasma treatment reduced the ZnO film and created oxygen vacancies in addition to form hydrogen donor level which decreased the crystallinity of the film.[53] Nitrogen plasma treatment decreased FWHM value slightly from 0.3639 to 0.3630 indicating nitrogen plasma's favorable effect on crystallinity of ZnO film. Nitrogen species from the plasma might have repaired some dangling bonds at the grain boundary and occupied some oxygen vacancies. FWHM of sample treated with all plasmas was 0.3634 which was even a little lower than the as deposited sample. Nitrogen species from the nitrogen plasma might fill the oxygen vacancies left behind by the hydrogen plasma treatment. Thus deterioration of crystallinity of ZnO film by hydrogen plasma could be substantially compensated by following nitrogen plasma treatment.

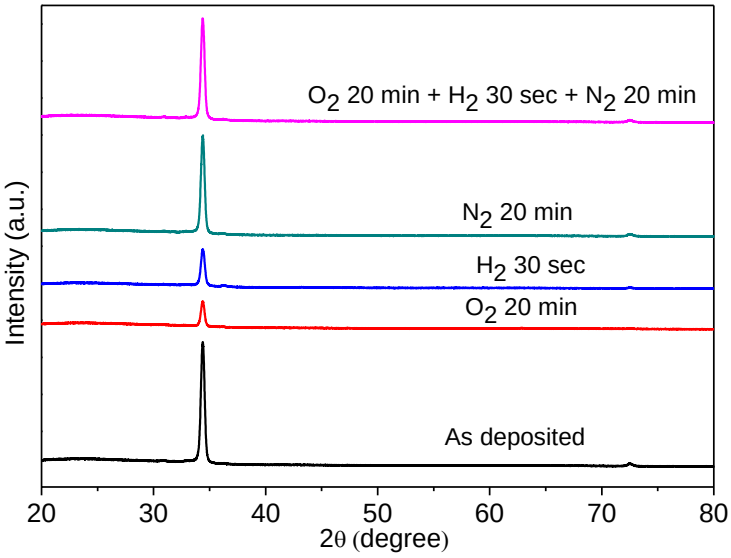

Figure 4.6. XRD intensity patterns of as-deposited, 20 min O_2, 30 sec H_2, 20 min N_2, and all plasma treated ZnO films.

Table 4.3. FWHM values of XRD peaks of oxygen, hydrogen, and nitrogen plasma treated ZnO films.

Plasma Conditions	As deposited	20 min O2	30 sec H2	20 min N2	20 min O2+ 30 sec H2+ 20 min N2
FWHM	0.3639	0.3567	0. 3695	0.3630	0.3634

4.1.3. Effect of plasma treatment on electrical parameters of ZnO films

The cause of n-type conductivity of undoped ZnO has been widely debated. It has been assumed for long time that oxygen vacancies in ZnO cause this n-type conductivity. But density functional calculations by Van de Walle and electron paramagnetic resonance (EPR) measurement by Hofmann et al. confirms that oxygen vacancies are deep donors

and cannot contribute to conductivity of ZnO [53, 55]. It has also been found that Zn interstitials and Zn antisites are also deep donors and cannot contribute to ZnO conductivity [89, 90]. Rather interstitial (H_i) and substitutional (H_O) hydrogens act as shallow donor and contribute to n-type conductivity of ZnO [53, 55]. Following results of this work is also supportive to hydrogen's contribution to the conductivity of ZnO.

Figure 4.7, Figure 4.8, and Figure 4.9 shows carrier concentration (n), Hall mobility (μ), and electrical resistivity (ρ) of as-deposited, 20 min O_2, 30 sec H_2, 20 min N_2, and all plasma treated ZnO films respectively. Figure 4.7 shows as deposited film had carrier concentration of 8.47E17 cm^{-3}. Plasma treatments increased carrier concentration except oxygen plasma treatment. Oxygen plasma treatment decreased n of as-deposited film to 2.53E17. Besides repairing grain boundaries, oxygen plasma oxidized the film and removed existing H_i and H_O donors which were incorporated to the film from organic compounds during growth, hence decreased the carrier concentration.

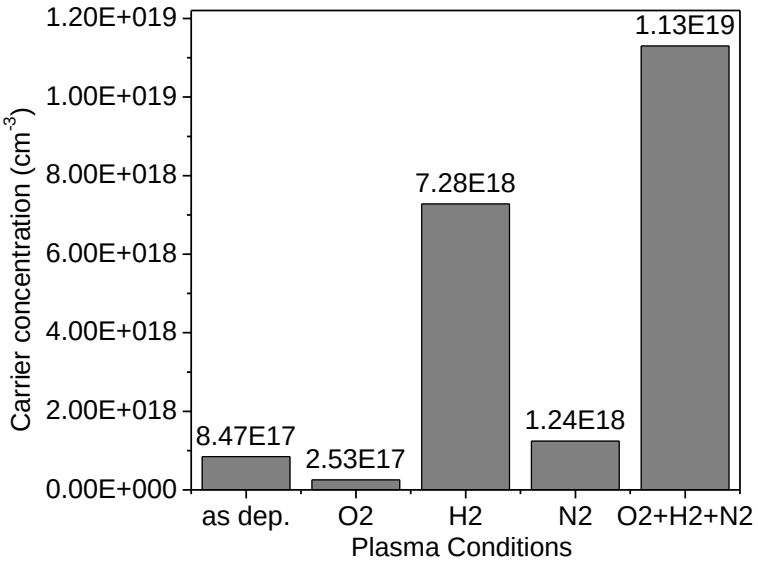

Figure 4.7. Carrier concentration (n) of as-deposited, 20 min O_2, 30 sec H_2, 20 min N_2, and all plasma treated ZnO film.

Repairing of grain boundaries of the film by oxygen plasma enabled easy drift of carrier through grain boundaries hence increased carrier mobility to 1.64 cm^2/ (V.s), shown in Figure 4.8. Again Figure 4.7 depicts that hydrogen treatment increased *n* almost by an order to 7.28E18 cm^{-3}. This large increase in *n* is attributed to formation of shallow hydrogen donor level immediately below the conduction band, significantly increasing the free carrier concentration [53, 54]. Besides forming H_i^+ and H_O^+ donor, hydrogen plasma also created some oxygen vacancies which was revealed by the increase in mobility to 23.3 cm^2/V/s (shown in Figure 4.8) resulting from decreased *O* scattering center. Nitrogen plasma treatment slightly increased both *n* and μ of the film which is ascribed to the removal of organic components and repairing defects. Sample treated with all three plasmas had highest *n* of 1.13E19 (shown in Figure 4.7) which resulted from combined favorable effects of hydrogen and nitrogen plasma treatment on carrier

concentration. Figure 4.8 depicts that all plasma treated sample had mobility of 6 cm^2/(V.s) which is way lower than the mobility of hydrogen plasma treated film. For all plasma treated sample, nitrogen species from nitrogen plasma filled up the oxygen vacancies left by preceding hydrogen plasma treatment hence introduced carrier scattering center and resulted decreased Hall mobility.

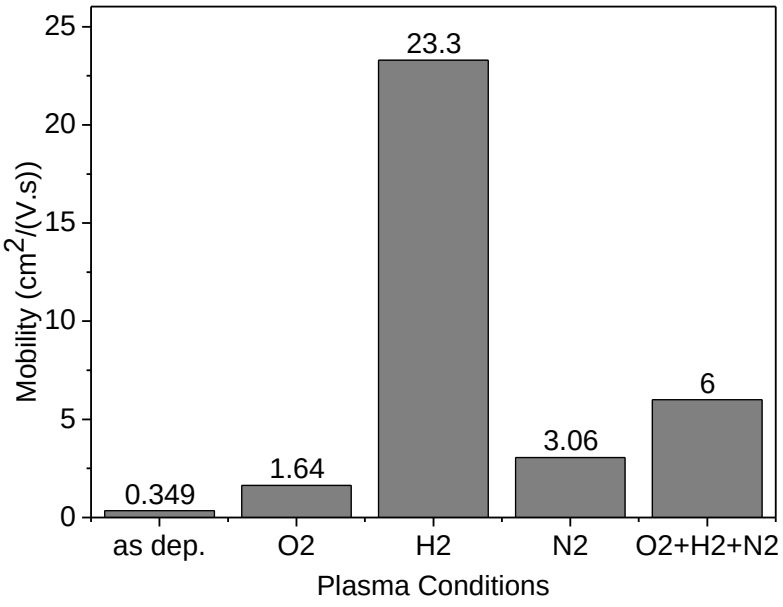

Figure 4.8. Hall mobility (μ) of as-deposited, 20 min O_2, 30 sec H_2, 20 min N_2, and all plasma treated ZnO film.

Figure 4.9 shows the effect of different plasma conditions on electrical resistivity of ZnO films. All conditions of plasma treatments decreased the resistivity of the ZnO film. Oxygen plasma treatment decreased the resistivity to 15 ohm-cm. Though the oxygen plasma treatment lowered carrier concentration (shown in Figure 4.7), increased mobility (shown in Figure 4.8) managed to reduce film's resistivity to some extent. Hydrogen plasma treated sample showed lowest resistivity of 0.0367 ohm-cm which was caused by

the increased mobility and carrier concentration. ZnO film treated sequentially with all three plasmas showed resistivity of 0.0367 ohm-cm which is 99.57% lower than the as deposited film.

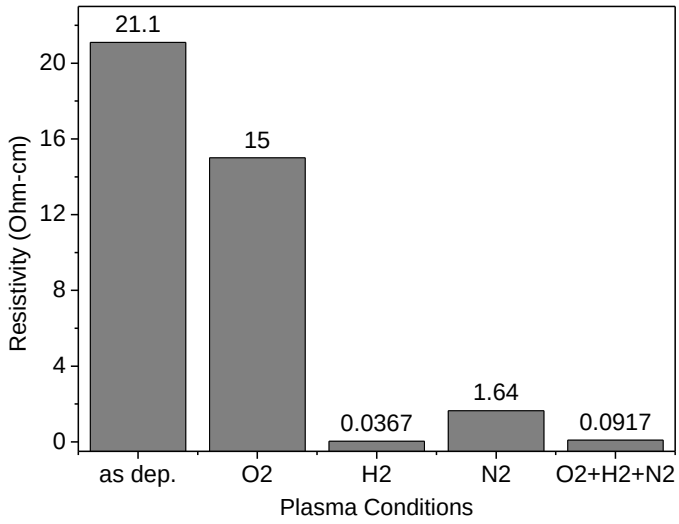

Figure 4.9. Resistivity of as-deposited, 20 min O_2, 30 sec H_2, 20 min N_2, and all plasma treated ZnO film.

4.2. Temperature sensing using zinc oxide thin film

4.2.1. Optical measurements for ZnO based temperature sensor

4.2.1.1. Absorption edge of zinc oxide thin film

Figure 4.10 illustrates transmittance spectra of the sol-gel derived ZnO film at different temperatures. A sharp absorption edge was observed between 370 nm and 400 nm wavelength. A red shift of the absorption edge was observed in the transmittance curves with increase of film's temperature. The red shift of ZnO films is attributed to the bandgap reduction of semiconductors and dielectrics at high temperature which can be explained by Varshni's empirical expression of Equation 1,

$$E_g(T) = E_g(0) - \frac{\alpha T^2}{T+\beta} \quad (1)$$

where, $E_g(0)$, α, and β are material's constants, and T is temperature. Other factors such as point defects in the ZnO thin film and temperature-induced change in band tail, temperature dependent stress/strain might also have contributed in redshift of transmission edge. In this work we considered application of uniform heating, such as radiation heating. An example is to measure the temperature in the center part of a vacuum system that is uniformly heated. Specifically, in our experiment, the ZnO coated glass was held on a slot of aluminum block and the central part of the ZnO film where light passed through was kept far away from the contact point. Thus the central part of the film was not expected to experience pronounced differential thermal expansion which might also affect the bandgap of ZnO film.

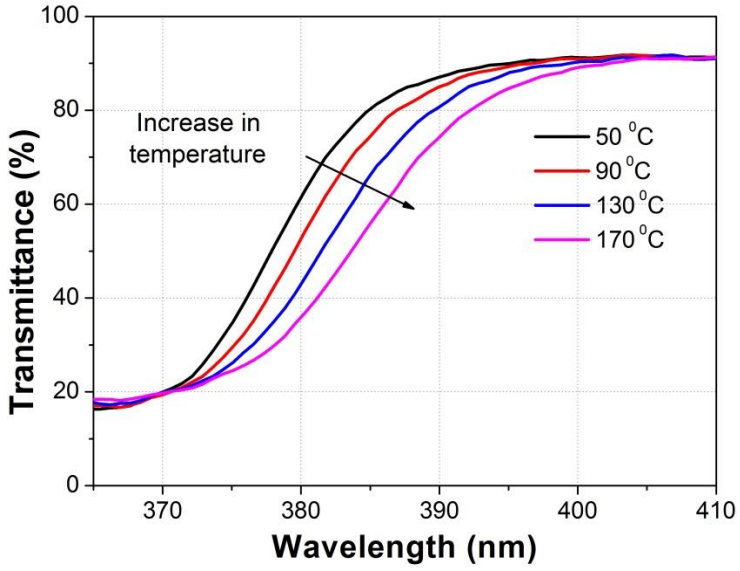

Figure 4.10. Transmittance versus wavelength of sol-gel derived ZnO film at different temperatures.

4.2.1.2. Absorption edge of glass substrate

Figure 4.11 shows transmittance spectra of bare glass substrate at different temperatures. The bare glass substrate also exhibited red shift of the absorption edge in between 270 nm and 360 nm, which was not so pronounced as the absorption edge films. Note that the absorption edge of the glass substrate did not overlap with that of the ZnO films. In the region of absorption edge of the ZnO films (i.e. 370–400 nm), the transmittance of glass remained almost constant at around 92% which allowed the ZnO film to dominate the change of transmittance of the ZnO coated glass in the film's absorption edge wavelength region.

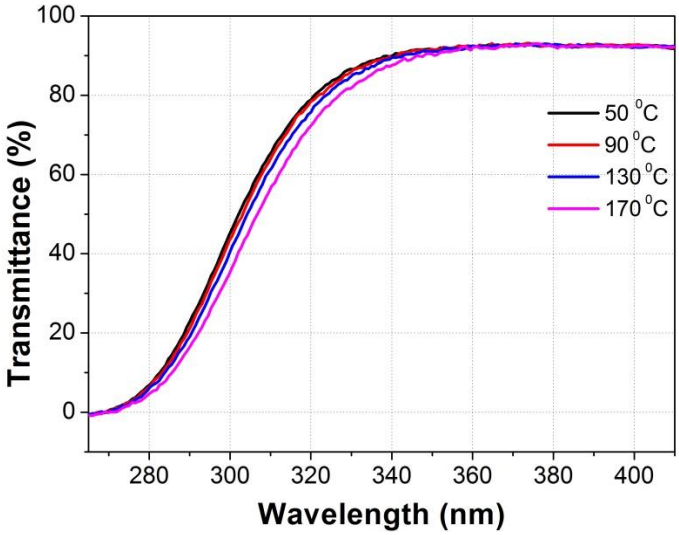

Figure 4.11. Transmittance versus wavelength of glass substrate at different temperatures.

4.2.1.3. Spectral Intensity distribution of the UV LED

Figure 4.12 shows normalized spectral intensity distribution of the UV LED used in the measurement. Peak intensity of the UV LED was found at 387 nm, which fell right

in the most sensitive region of the ZnO absorption edge. The UV LED radiated optical power mostly in the wave length range from 370 nm to 420 nm.

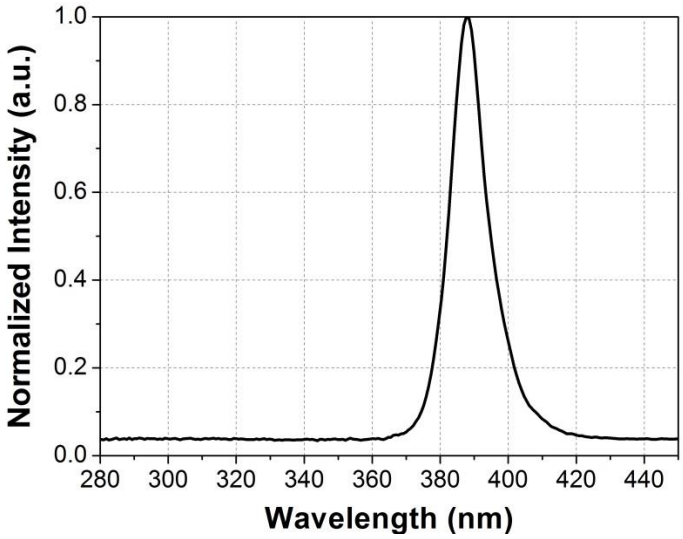

Figure 4.12. Normalized spectral intensity distribution of the UV LED light source.

4.2.2. Temperature sensing using ZnO film

The ZnO coated sample was maintained at different temperatures using the temperature controller and corresponding photodiode's short circuit current was measured. The temperature was varied from 50 to 310 °C. Figure 4.13 shows photodiode response at various temperatures for the ZnO coated glass and bare glass substrate. The short circuit current of photodiode decreased linearly as the temperature of the ZnO coated glass increased, which resulted from the shifting of absorption edge of ZnO toward longer wavelength. The photodiode current decreased by 24.99 µA from 74 µA to 49.01 µA as the temperature of ZnO coated glass was increased from 50 °C to 310 °C. Photocurrent decreased by 33.77% for the ZnO coated glass in measured temperature range. Linear regression line along with the equation of the response photocurrent

obtained by Microsoft Excel tool has also been shown in Figure 4.13. The linear trend-line indicated a negative slope of 0.0973 µA/°C and R-square value of 0.996 which was very close to unity. The bare glass substrate resulted in a slight and slow decrease in the photo-current. Photocurrent decreased by 1.59 µA from 74.89 µA to 73.30 µA as the temperature of glass substrate was increased from 50 °C to 310 °C. Photocurrent decreased by only 2.12% for the glass substrate in measured temperature range. This decrease in photo current was mainly attributed to the disturbed and inferior focusing of light on photodiode at raised temperature caused by heat haze: an inferior transmission of light through hot air due to temperature and refractive index gradient. So, the linear decrease in photocurrent for ZnO coated glass was caused by the red-shift of absorption edge of ZnO film. Thus, the ZnO coated glass can be used for an optical temperature sensing system. The experimental result indicated a temperature coefficient of ~0.1 µA/°C.

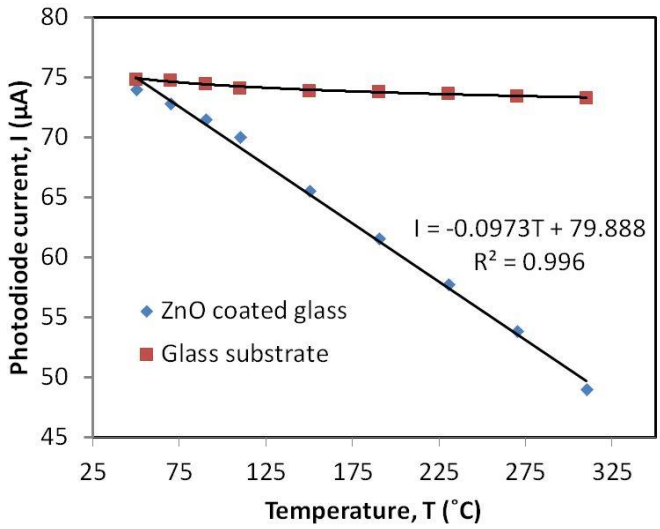

Figure 4.13. Photodiode current at varying temperature for ZnO coated glass and glass substrate.

4.2.3. ZnO film's structural and morphological property before and after test

4.2.3.1. XRD measurement of ZnO film before and after test

X-ray diffraction measurements were performed on ZnO films before and after the temperature measurement to verify its thermal stability. Figure 4.14 shows XRD patterns of the as-prepared and tested ZnO films. The observed peak positions were 34.41° and 34.39° with full width half maximum (FWHM) of 0.41° and 0.40° for the as-prepared and tested samples, respectively. The single diffraction peak at 34.4° corresponding to (002) crystallographic plane indicated a strong preferred orientation of the ZnO crystal structure. The XRD results confirmed good thermal stability of the sol-gel ZnO films, which were suitable for temperature sensing.

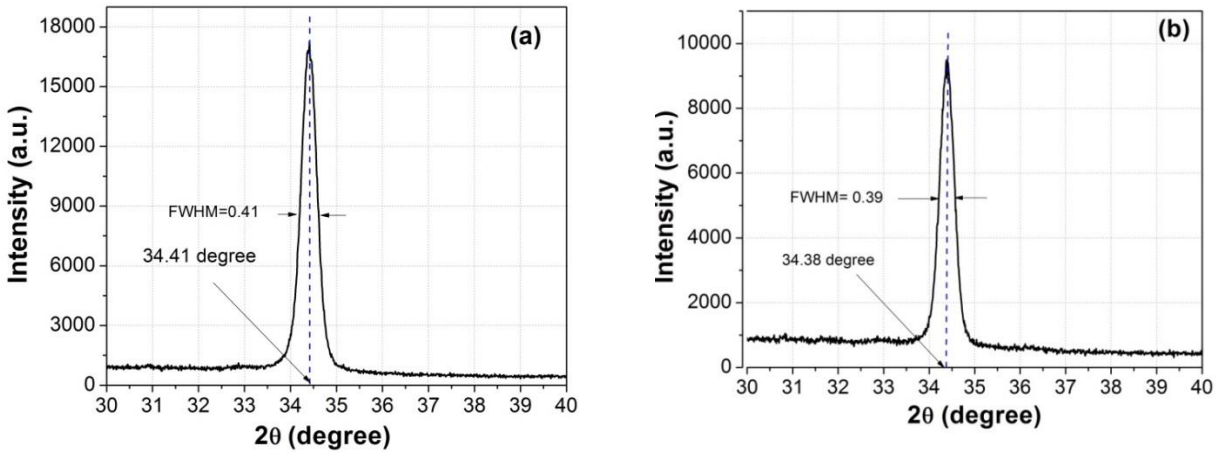

Figure 4.14. XRD pattern of a ZnO thin film: (a) as-prepared and (b) tested at 310°C.

4.2.3.2. AFM topography of ZnO film before and after test

Figure 4.15 shows 2D and 3D AFM topography of the as-prepared and tested ZnO thin films. Surface roughness was 3.71 and 2.97 nm for the as-prepared and tested

ZnO thin films, respectively. Testing of the films as sensing element did not worsen or roughen the surface, which made the film re-usable for temperature sensing.

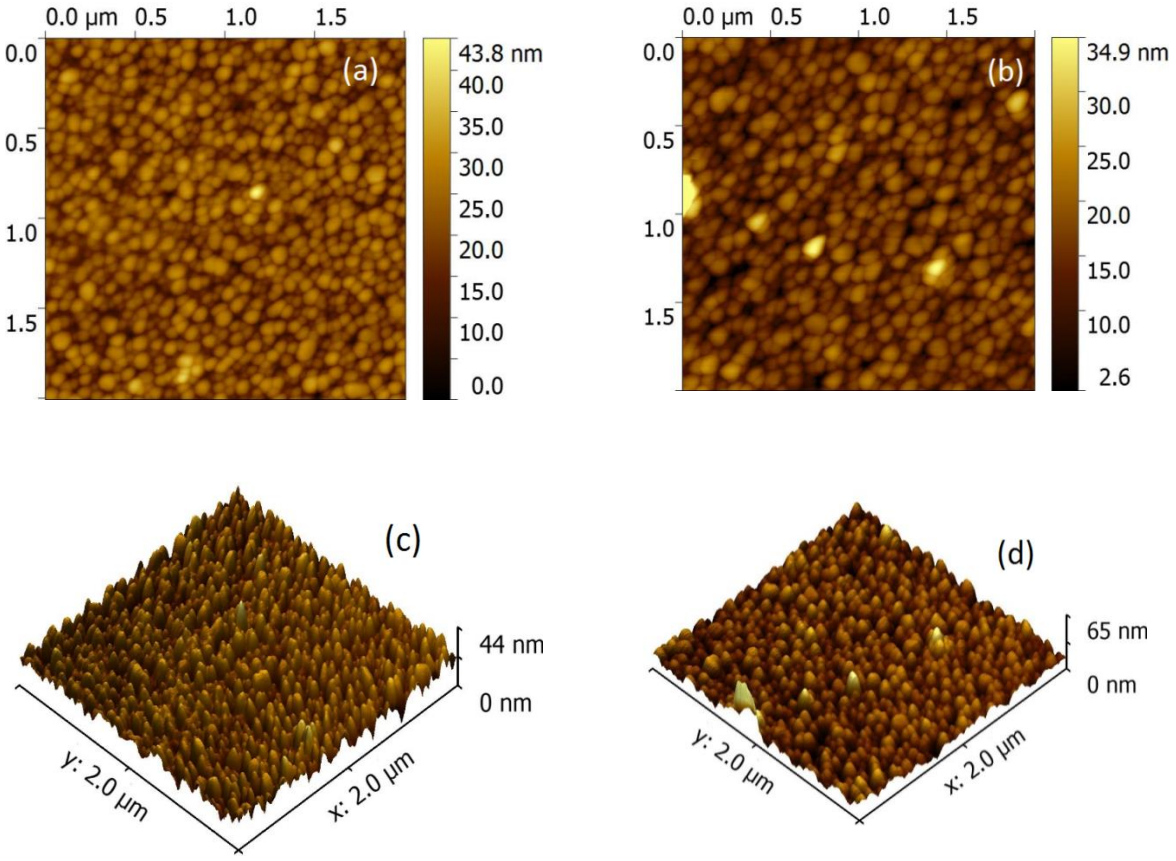

Figure 4.15. AFM 2D topography of (a) as prepared (b) tested at 310 °C, AFM 3D topography of (c) as prepared, and (d) tested at 310 °C.

CHAPTER 5. CONCLUSIONS

5.1. Summary

Zinc oxide is a group II-VI semiconductor with direct and wide bandgap of 3.37 eV at room temperature. ZnO is a promising material for UV optoelectronic application for its direct-wide bandgap. Its large exciton binding energy of 60 meV enables applications in exciton effect based optical devices. Zinc oxide is also a promising material for transparent conductive oxide (TCO) for LCD, OLED displays, thin film solar cells, and touch screens. ZnO is more advantageous material over other TCOs such as ITO, FTO, and CdO:In for its availability, low cost, non-toxicity, and suitable optical and structural property.

Zinc oxide thin films are mostly grown by various costly vacuum based fabrication method. Solution-based sol-gel deposition of ZnO thin films has been reported as a simple, easy and low-cost method. Sol-gel derived nanocrystalline zinc oxide thin films suffer from relatively poor electrical and optical properties. Finding ways to improve electrical and optical properties of sol-gel processed zinc oxide has been seeking attention of researchers. So, there is a need for improved electrical properties of sol-gel derived zinc oxide thin film maintaining good optical and structural properties.

Most temperature measurement system requires physical and/or electrical contact between the main sensing element and supporting parts of the measurement system. In many applications, such electrical feedthrough is not allowed or not convenient. Hence, optical measurement of temperature which does not require electrical feedthrough is

needed. Temperature dependent red-shift property of ZnO film makes it as an attractive material for optical temperature sensing.

ZnO oxide thin films were fabricated on glass substrate from zinc acetate dihydrate, 2-methoxethanol and ethanolamine via sol-gel spin coating method. To improve electrical and optical properties, the samples were treated with oxygen, hydrogen and nitrogen plasma. Optical transmittance, crystallinity, surface morphology, and electrical parameters of the ZnO films were characterized by Filmetrics F-20 spectrophotometer, Rigaku Smartlab x-ray diffractometer, Bruker Dimension Icon AFM, and Ecopia Hall Effect measurement system respectively. Moreover, an optical temperature sensor was then established using the ZnO coated glass as sensing element, ultra-violet (UV) light emitting diode (LED) as light source, and a UV photodiode as light detector.

The average transmittance over visible wavelength range for the as-deposited ZnO film, oxygen plasma treated film, and nitrogen plasma treated film were 82%, 81.3% and 81.2%, respectively. Hydrogen plasma treated sample had the lowest transmittance having average value of 76.7% in visible wavelength spectrum. Treatment with all three plasmas sequentially resulted in much higher transmittance than hydrogen plasma treated sample. The average transmittance over visible wavelength range for the sequential plasma treated sample was 79.8%. Nitrogen plasma treatment following hydrogen plasma led to recovery of the adverse effect on transmittance by hydrogen plasma.

Crystallinity of the films was revealed by FWHM values. The as-deposited film had FWHM value of 0.3639. Oxygen treated ZnO film had the lowest FWHM value of 0.3567 which indicated better crystallinity. Hydrogen plasma treatment increased the FWHM value to 0. 3695, which indicated reduced crystallinity. Nitrogen plasma treatment decreased FWHM value slightly from 0.3639 to 0.3630 indicating nitrogen plasma's favorable effect on crystallinity of ZnO film. FWHM of sample treated with the three plasmas was 0.3634, which was even a little lower than the as-deposited sample. Thus, deterioration of crystallinity of ZnO film by hydrogen plasma could be substantially compensated by the nitrogen plasma treatment.

Previous theoretical and experimental investigation confirmed interstitial (H_i) and substitutional (H_O) hydrogens contribution toward n-type conductivity of ZnO. The as-deposited film had carrier concentration of 8.47E17 cm^{-3} mobility of 0.349 cm^2/ (V.s). Plasma treatments increased carrier concentration except oxygen plasma treatment, which led to decreased n of 2.53E17 cm^{-3}. Oxygen plasma treatment increased carrier mobility to 1.64 cm2/ (V.s). Hydrogen treatment increased carrier concentration almost by an order to 7.28E18 cm^{-3} and led to the increased mobility of 23.3 cm^2/ (V.s). The sample treated in sequence with the three plasmas had highest carrier concentration of 1.13E19 cm^{-3} mobility of 6 cm^2/ (V.s). Sequential oxygen-hydrogen-nitrogen plasma treatment resulted in resistivity of 0.0367 ohm-cm, which was over two orders lower than the as-deposited film

Transmittance spectra of the sol-gel derived ZnO film was measured at different temperatures. A sharp absorption edge was observed between 370 nm and 400 nm

wavelength. A red shift of the absorption edge was observed in the transmittance curves with increase of film's temperature. For realizing an optical temperature sensing system, ZnO coated glass sample was used as main sensing element. The temperature measurement system was tested for temperature range of 50 - 310 °C. Short circuit current of photodiode decreased linearly as the temperature of the ZnO coated glass was increased. The photodiode's current reduced by 24.8 μA for the ZnO coated glass as the sample temperature was increased from 50 °C to 310 °C.

5.2. Conclusions

Nanocrystalline zinc oxide thin films were fabricated by a solution-based process and treated with oxygen, hydrogen, and nitrogen plasmas. The as-deposited films had resistivity of 21.1 Ohm-cm and transmittance of 82%. Oxygen plasma could repair defects and increased the crystallinity of the film. Hydrogen plasma treatment introduced hydrogen donors resulting in high carrier density and oxygen vacancies that led to increased carrier mobility. Hydrogen plasma reduced the transmittance of the ZnO films to 76.7%. Sequential plasma treatment (oxygen-hydrogen-nitrogen) greatly reduced the ZnO film resistivity by more than two orders, while the average transmittance in visible range remained close to the as-deposited film of ~80%. Optical bandgap of sol-gel derived ZnO thin films exhibited strong temperature dependence. The bandgap narrowing was evidenced by pronounced red-shift of the optical absorption edge with increasing temperature. Optical temperature sensing could be realized based on the absorption of the ZnO thin films using an ultra-violet light emitting diode of 380 nm center wavelength and a UV photo-detector. The photo-current detected by the photo-diode decreased linearly with the increase in the temperature of the ZnO film. The ZnO thin film based optical

temperature sensing can be engineered and customized for various applications where conventional sensor is not feasible and/or IR thermometry does not give satisfactory performance.

5.3. Future work

Nitrogen plasma treatment can be adopted to achieve p-type conductivity of zinc oxide film which is still a big challenge in the research of ZnO material. Further modification to the temperature sensor such as using a reference detector can be implemented to overcome the instability of the power supply and UV light source.

REFERENCES

[1] Ü. Özgür, Y. I. Alivov, C. Liu, A. Teke, M. Reshchikov, S. Doğan, *et al.*, "A comprehensive review of ZnO materials and devices," *Journal of Applied Physics,* vol. 98, p. 041301, 2005.

[2] A. Mang and K. Reimann, "Band gaps, crystal-field splitting, spin-orbit coupling, and exciton binding energies in ZnO under hydrostatic pressure," *Solid State Communications,* vol. 94, pp. 251-254, 1995.

[3] D. C. Reynolds, D. C. Look, and B. Jogai, "Optically pumped ultraviolet lasing from ZnO," *Solid State Communications,* vol. 99, pp. 873-875, 1996.

[4] D. Bagnall, Y. Chen, Z. Zhu, T. Yao, S. Koyama, M. Y. Shen, *et al.*, "Optically pumped lasing of ZnO at room temperature," *Applied Physics Letters*, vol. 70, pp. 2230-2232, 1997.

[5] D. C. Look, "Recent advances in ZnO materials and devices," *Materials Science and Engineering: B,* vol. 80, pp. 383-387, 2001.

[6] H. Nanto, H. Sokooshi, and T. Usuda, "Smell sensor using zinc oxide thin films prepared by magnetron sputtering," *International Conference on Solid-State Sensors and Actuators, ,* pp. 596-599, *1991*.

[7] M. Caglar, Y. Caglar, S. Aksoy, and S. Ilican, "Temperature dependence of the optical band gap and electrical conductivity of sol–gel derived undoped and Li-doped ZnO films," *Applied Surface Science,* vol. 256, pp. 4966-4971, 2010.

[8] V. Srikant and D. R. Clarke, "On the optical band gap of zinc oxide," *Journal of Applied Physics,* vol. 83, pp. 5447-5451, 1998.

[9] S. S. H.-M. Kim, "Transparent Conductive Oxide (TCO) Films for Organic Light Emissive Devices (OLEDs)."

[10] D. M. Mattox and V. H. Mattox, "Review of Transparent Conductive Oxides (TCO)."

[11] A. Stadler, "Transparent conducting oxides—An up-to-date overview," *Materials,* vol. 5, pp. 661-683, 2012.

[12] T. J. Coutts, T. O. Mason, J. Perkins, and D. S. Ginley, "Transparent conducting oxides: status and opportunities in basic research," in *Photovoltaics for the 21st Century: Proceedings of the International Symposium*, 1999, pp. 274-286.

[13] R. G. Gordon, "Criteria for choosing transparent conductors," *MRS bulletin,* vol. 25, pp. 52-57, 2000.

[14] K. Minegishi, Y. Koiwai, Y. Kikuchi, K. Yano, M. Kasuga, and A. Shimizu, "Growth of p-type zinc oxide films by chemical vapor deposition," *Japanese Journal of Applied Physics,* vol. 36, p. L1453, 1997.

[15] H. Nanto, T. Minami, S. Shooji, and S. Takata, "Electrical and optical properties of zinc oxide thin films prepared by rf magnetron sputtering for transparent electrode applications," *Journal of Applied Physics,* vol. 55, pp. 1029-1034, 1984.

[16] D. C. Look, D. Reynolds, C. Litton, R. Jones, D. Eason, and G. Cantwell, "Characterization of homoepitaxial p-type ZnO grown by molecular beam epitaxy," *Applied Physics Letters,* vol. 81, pp. 1830-1832, 2002.

[17] S. L. King, J. Gardeniers, and I. W. Boyd, "Pulsed-laser deposited ZnO for device applications," *Applied Surface Science,* vol. 96, pp. 811-818, 1996.

[18] T. Ive, T. Ben-Yaacov, C. G. Van de Walle, U. K. Mishra, S. P. DenBaars, and J. S. Speck, "Step-flow growth of ZnO(0 0 0 1) on GaN(0 0 0 1) by metalorganic chemical vapor epitaxy," *Journal of Crystal Growth,* vol. 310, pp. 3407-3412, 7/15/ 2008.

[19] T. Ive, T. Ben-Yaacov, A. Murai, H. Asamizu, C. G. Van de Walle, U. Mishra, *et al.*, "Metalorganic chemical vapor deposition of ZnO(0001) thin films on GaN(0001) templates and ZnO(0001) substrates," *Physica Status Solidi (c),* vol. 5, pp. 3091-3094, 2008.

[20] S. Heinze, A. Krtschil, J. Bläsing, T. Hempel, P. Veit, A. Dadgar, *et al.*, "Homoepitaxial growth of ZnO by metalorganic vapor phase epitaxy in two-dimensional growth mode," *Journal of Crystal Growth,* vol. 308, pp. 170-175, 10/1/ 2007.

[21] Y. Natsume and H. Sakata, "Zinc oxide films prepared by sol-gel spin-coating," *Thin Solid Films,* vol. 372, pp. 30-36, 9/1/ 2000.

[22] S. A. Kamaruddin, K.-Y. Chan, H.-K. Yow, M. Zainizan Sahdan, H. Saim, and D. Knipp, "Zinc oxide films prepared by sol–gel spin coating technique," *Applied Physics A,* vol. 104, pp. 263-268, 2011.

[23] H. Li, J. Wang, H. Liu, H. Zhang, and X. Li, "Zinc oxide films prepared by sol–gel method," *Journal of Crystal Growth,* vol. 275, pp. e943-e946, 2/15/ 2005.

[24] C.-Y. Tsay, K.-S. Fan, Y.-W. Wang, C.-J. Chang, Y.-K. Tseng, and C.-K. Lin, "Transparent semiconductor zinc oxide thin films deposited on glass substrates by sol–gel process," *Ceramics International,* vol. 36, pp. 1791-1795, 8// 2010.

[25] D. Bao, H. Gu, and A. Kuang, "Sol-gel-derived c-axis oriented ZnO thin films," *Thin Solid Films,* vol. 312, pp. 37-39, 1/14/ 1998.

[26] M. N. Kamalasanan and S. Chandra, "Sol-gel synthesis of ZnO thin films," *Thin Solid Films,* vol. 288, pp. 112-115, 11/15/ 1996.

[27] M. Ohyama, H. Kouzuka, and T. Yoko, "Sol-gel preparation of ZnO films with extremely preferred orientation along (002) plane from zinc acetate solution," *Thin Solid Films,* vol. 306, pp. 78-85, 1997.

[28] H. Li, J. Wang, H. Liu, C. Yang, H. Xu, X. Li, *et al.*, "Sol–gel preparation of transparent zinc oxide films with highly preferential crystal orientation," *Vacuum,* vol. 77, pp. 57-62, 12/17/ 2004.

[29] K. R. Murali, "Properties of sol–gel dip-coated zinc oxide thin films," *Journal of Physics and Chemistry of Solids,* vol. 68, pp. 2293-2296, 12// 2007.

[30] M. Vafaee and M. S. Ghamsari, "Preparation and characterization of ZnO nanoparticles by a novel sol–gel route," *Materials Letters,* vol. 61, pp. 3265-3268, 6// 2007.

[31] L. Znaidi, G. J. A. A. Soler Illia, S. Benyahia, C. Sanchez, and A. V. Kanaev, "Oriented ZnO thin films synthesis by sol–gel process for laser application," *Thin Solid Films,* vol. 428, pp. 257-262, 3/20/ 2003.

[32] G. Srinivasan and J. Kumar, "Optical and structural characterisation of zinc oxide thin films prepared by sol-gel process," *Crystal Research and Technology,* vol. 41, pp. 893-896, 2006.

[33] J.-H. Lee, K.-H. Ko, and B.-O. Park, "Electrical and optical properties of ZnO transparent conducting films by the sol–gel method," *Journal of Crystal Growth,* vol. 247, pp. 119-125, 2003.

[34] Y. Natsume and H. Sakata, "Electrical and optical properties of zinc oxide films post-annealed in H2 after fabrication by sol–gel process," *Materials Chemistry and Physics,* vol. 78, pp. 170-176, 2/3/ 2003.

[35] Y.-S. Kim, W.-P. Tai, and S.-J. Shu, "Effect of preheating temperature on structural and optical properties of ZnO thin films by sol–gel process," *Thin Solid Films,* vol. 491, pp. 153-160, 11/22/ 2005.

[36] S. Bandyopadhyay, G. K. Paul, R. Roy, S. K. Sen, and S. Sen, "Study of structural and electrical properties of grain-boundary modified ZnO films prepared by sol–gel technique," *Materials Chemistry and Physics,* vol. 74, pp. 83-91, 2/1/ 2002.

[37] S. Walther, S. Polster, M. Jank, H. Thiem, H. Ryssel, and L. Frey, "Tuning of charge carrier density of ZnO nanoparticle films by oxygen plasma treatment," *Advanced Powder Technology,* vol. 22, pp. 253-256, 2011.

[38] M. Morales-Masis, L. Ding, F. Dauzou, Q. Jeangros, A. Hessler-Wyser, S. Nicolay, *et al.*, "Hydrogen plasma treatment for improved conductivity in amorphous aluminum doped zinc tin oxide thin films," *APL Materials,* vol. 2, p. 096113, 2014.

[39] S. Major, S. Kumar, M. Bhatnagar, and K. Chopra, "Effect of hydrogen plasma treatment on transparent conducting oxides," *Applied Physics Letters,* vol. 49, pp. 394-396, 1986.

[40] J. Roth, "Industrial Plasma Engineering Volume 1 Principles. Bristol and Philadelphia," ed: Institute of Physics publishing, 1995.

[41] T. Makabe and Z. L. Petrovic, *Plasma electronics: applications in microelectronic device fabrication* vol. 26: CRC Press, 2014.

[42] F.-L. Kuo, Y. Li, M. Solomon, J. Du, and N. D. Shepherd, "Workfunction tuning of zinc oxide films by argon sputtering and oxygen plasma: an experimental and computational study," *Journal of Physics D: Applied Physics,* vol. 45, p. 065301, 2012.

[43] Y. Chen, D. Bagnall, H.-j. Koh, K.-t. Park, K. Hiraga, Z. Zhu, *et al.*, "Plasma assisted molecular beam epitaxy of ZnO on c-plane sapphire: growth and characterization," *Journal of Applied Physics,* vol. 84, pp. 3912-3918, 1998.

[44] T. W. Kerlin and M. Johnson, *Practical Thermocouple Thermometry*: Instrument Society of America, 1999.

[45] E. O. Doebelin, *Measurement systems: application and design* vol. 4: McGraw-Hill New York, 1990.

[46] T. Barry, G. Fuller, K. Hayatleh, and J. Lidgey, "Self-calibrating infrared thermometer for low-temperature measurement," *Instrumentation and Measurement, IEEE Transactions on,* vol. 60, pp. 2047-2052, 2011.

[47] K. P. O'Donnell and X. Chen, "Temperature dependence of semiconductor band gaps," *Applied Physics Letters,* vol. 58, pp. 2924-2926, 1991.

[48] A. Janotti and C. G. Van de Walle, "Fundamentals of zinc oxide as a semiconductor," *Reports on Progress in Physics,* vol. 72, p. 126501, 2009.

[49] J. Pokharel, M. Shrestha, L. Q. Zhou, V. Neto, and Q. H. Fan, "Oriented Zinc Oxide Nanocrystalline Thin Films Grown from Sol-Gel Solution," *Journal of Coating Science and Technology,* vol. 2, pp. 46-50, 2015.

[50] P. Cai, D. Zhen, X. Xu, Y. Liu, N. Chen, G. Wei, *et al.*, "A novel fiber-optic temperature sensor based on high temperature-dependent optical properties of ZnO film on sapphire fiber-ending," *Materials Science and Engineering: B,* vol. 171, pp. 116-119, 2010.

[51] K. J. Hong and T. S. Jeong, "Growth and optical absorption spectra of ZnO films grown by pulsed laser deposition," *Journal of Crystal Growth,* vol. 280, pp. 545-550, 2005.

[52] M. Wang, E. J. Kim, J. S. Chung, E. W. Shin, S. H. Hahn, K. E. Lee, *et al.*, "Influence of annealing temperature on the structural and optical properties of sol–gel prepared ZnO thin films," *Physica Status Solidi (a),* vol. 203, pp. 2418-2425, 2006.

[53] C. G. Van de Walle, "Hydrogen as a Cause of Doping in Zinc Oxide," *Physical Review Letters,* vol. 85, pp. 1012-1015, 07/31/ 2000.

[54] A. K. Singh, A. Janotti, M. Scheffler, and C. G. Van de Walle, "Sources of Electrical Conductivity in SnO_2" *Physical Review Letters,* vol. 101, p. 055502, 07/31/ 2008.

[55] D. M. Hofmann, A. Hofstaetter, F. Leiter, H. Zhou, F. Henecker, B. K. Meyer, *et al.*, "Hydrogen: A Relevant Shallow Donor in Zinc Oxide," *Physical Review Letters*, vol. 88, p. 045504, 01/10/ 2002.

[56] Z. Zhou, K. Kato, T. Komaki, M. Yoshino, H. Yukawa, M. Morinaga, *et al.*, "Effects of dopants and hydrogen on the electrical conductivity of ZnO," *Journal of the European Ceramic Society*, vol. 24, pp. 139-146, 2004.

[57] T. M. Barnes, K. Olson, and C. A. Wolden, "On the formation and stability of p-type conductivity in nitrogen-doped zinc oxide," *Applied Physics Letters*, vol. 86, p. 2112, 2005.

[58] M. Morales-Masis, L. Ding, F. Dauzou, Q. Jeangros, A. Hessler-Wyser, S. Nicolay, *et al.*, "Hydrogen plasma treatment for improved conductivity in amorphous aluminum doped zinc tin oxide thin films," *APL Mater.*, vol. 2, p. 096113, 2014.

[59] H. Wang, A. Yang, and L. Tang, "Wide measurement-range fiber-optic temperature sensor based on ZnO thin film," *Optics and Lasers in Engineering*, vol. 60, pp. 49-53, 2014.

[60] "Transparent conductive oxides," *Available at: http://www.omegafilters.com/capabilities/transparent-conductive-oxides/, Last accessed: 08/01/2016*.

[61] S. E. Harrison, "Conductivity and Hall Effect of ZnO at Low Temperatures," *Physical Review*, vol. 93, pp. 52-62, 01/01/ 1954.

[62] K. Hoffmann and D. Hahn, "Electron Spin Resonance of Lattice Defects in Zinc Oxide," *Physica Status Solidi (a)*, vol. 24, pp. 637-648, 1974.

[63] A. R. Hutson, "Hall Effect Studies of Doped Zinc Oxide Single Crystals," *Physical Review*, vol. 108, pp. 222-230, 10/15/ 1957.

[64] K. I. Hagemark, "Defect structure of Zn-doped ZnO," *Journal of Solid State Chemistry*, vol. 16, pp. 293-299, 1976/01/15 1976.

[65] H. Kato, M. Sano, K. Miyamoto, and T. Yao, "Growth and characterization of Ga-doped ZnO layers on a-plane sapphire substrates grown by molecular beam epitaxy," *Journal of Crystal Growth*, vol. 237–239, Part 1, pp. 538-543, 4// 2002.

[66] A. Tsukazaki, A. Ohtomo, T. Onuma, M. Ohtani, T. Makino, M. Sumiya, *et al.*, "Repeated temperature modulation epitaxy for p-type doping and light-emitting diode based on ZnO," *Nat Mater*, vol. 4, pp. 42-46, 01//print 2005.

[67] D. C. Look, D. C. Reynolds, C. W. Litton, R. L. Jones, D. B. Eason, and G. Cantwell, "Characterization of homoepitaxial p-type ZnO grown by molecular beam epitaxy," *Applied Physics Letters*, vol. 81, pp. 1830-1832, 2002.

[68] E. S. Tuzemen, K. Kara, S. Elagoz, D. K. Takci, I. Altuntas, and R. Esen, "Structural and electrical properties of nitrogen-doped ZnO thin films," *Applied Surface Science*, vol. 318, pp. 157-163, 2014.

[69] C. J. Brinker and G. W. Scherer, *Sol-gel science: the physics and chemistry of sol-gel processing*: Academic press, 2013.

[70] L. Znaidi, "Sol–gel-deposited ZnO thin films: a review," *Materials Science and Engineering: B,* vol. 174, pp. 18-30, 2010.

[71] D. Meyerhofer, "Characteristics of resist films produced by spinning," *Journal of Applied Physics,* vol. 49, pp. 3993-3997, 1978.

[72] A. G. Emslie, F. T. Bonner, and L. G. Peck, "Flow of a Viscous Liquid on a Rotating Disk," *Journal of Applied Physics,* vol. 29, pp. 858-862, 1958.

[73] H. F. Dam, "Spin coating," *Available: http://plasticphotovoltaics.org/lc/lc-fabrication/lc-coating/lc-spin.html, Last accessed: 08/01/2016*.

[74] T. Ivanova, A. Harizanova, T. Koutzarova, and B. Vertruyen, "Study of ZnO sol–gel films: Effect of annealing," *Materials Letters,* vol. 64, pp. 1147-1149, 5/31/ 2010.

[75] S.-Y. Kuo, W.-C. Chen, and C.-P. Cheng, "Investigation of annealing-treatment on the optical and electrical properties of sol–gel-derived zinc oxide thin films," *Superlattices and Microstructures,* vol. 39, pp. 162-170, 2006.

[76] R. Castanedo-Pérez, O. Jiménez-Sandoval, S. Jiménez-Sandoval, J. Márquez-Marín, A. Mendoza-Galván, G. Torres-Delgado, *et al.*, "Influence of annealing temperature on the formation and characteristics of sol-gel prepared ZnO films," *Journal of Vacuum Science & Technology A,* vol. 17, pp. 1811-1816, 1999.

[77] Z.-N. Ng, K.-Y. Chan, and T. Tohsophon, "Effects of annealing temperature on ZnO and AZO films prepared by sol–gel technique," *Applied Surface Science,* vol. 258, pp. 9604-9609, 10/1/ 2012.

[78] M. Wang, J. Wang, W. Chen, Y. Cui, and L. Wang, "Effect of preheating and annealing temperatures on quality characteristics of ZnO thin film prepared by sol–gel method," *Materials Chemistry and Physics,* vol. 97, pp. 219-225, 2006.

[79] J. Webster, *Medical instrumentation: application and design*: John Wiley & Sons, 2009.

[80] F. O. Garces, "UV Visible Absorption Spectroscopy," *Available: http://faculty.sdmiramar.edu/fgarces/LabMatters/Instruments/UV_Vis/Cary50.htm, Last accessed: 08/01/2016*.

[81] B. Fultz and J. M. Howe, *Transmission electron microscopy and diffractometry of materials*: Springer Science & Business Media, 2012.

[82] B. D. Cullity, "Elements of X-ray Diffraction," 2001.

[83] "Available at: https://en.wikipedia.org/wiki/Hall_effect," *Last accessed: 08/01/2016.*

[84] R. Green, "Hall Effect Measurements in Materials Characterization," *White paper,* 2011, Available:

http://www.tek.com/sites/tek.com/files/media/document/resources/HallEffect_WhtPapr.pdf, Last accessed 08/01/2016.

[85] W. R. Thurber, "Hall Effect Measurements," *Available: http://www.nist.gov/pml/div683/hall.cfm, Last accessed: 08/01/2016.*

[86] P. Eaton and P. West, *Atomic force microscopy*: Oxford University Press, 2010.

[87] A. Hall, "An introduction to atomic force microscopy," *Avaiable: https://amyhallr.wordpress.com/2013/03/15/atomic-force-microscopy/, Last accessed: 08/01/2016.*

[88] Q. Qiao, "Lecture Slides-X-ray Diffraction: EE 560 Sensors and Measurement," 2015.

[89] A. Janotti and C. G. Van de Walle, "New insights into the role of native point defects in ZnO," *Journal of Crystal Growth,* vol. 287, pp. 58-65, 1/18/ 2006.

[90] A. Janotti and C. G. Van de Walle, "Native point defects in ZnO," *Physical Review B,* vol. 76, p. 165202, 10/04/ 2007.